

## RESERVOIR SANDSTONES OF THE CRETACEOUS NAPO FORMATION U AND T MEMBERS IN THE ORIENTE BASIN, ECUADOR: LINKS BETWEEN DIAGENESIS AND SEQUENCE STRATIGRAPHY

J. Estupiñan<sup>1</sup>\*, R. Marfil<sup>2</sup>, M. Scherer<sup>3</sup> and A. Permanyer<sup>4</sup>

*This paper investigates whether diagenetic alterations in sandstones and resulting changes in reservoir quality are influenced by depositional environments and sequence stratigraphy. The study focusses on the Cretaceous U and T sandstone members of the Napo Formation in the Oriente Basin of Ecuador. The sandstones were deposited in fluvial, transitional and marine environments, and comprise Lowstand (LST), Transgressive (TST) and Highstand Systems Tract (HST) deposits. The data were obtained by detailed petrographic observations supported by microprobe, stable isotope, and fluid inclusion analyses. The sandstones consist of fine- to medium-grained quartzarenites and subarkoses. Diagenetic events include cementation by chlorite, early and late kaolinite/dickite, early and late carbonates (siderite, Fe-dolomite/ankerite), and quartz.*

*Early (eogenetic) processes included formation of chlorite grain coatings, kaolinite pore filling, and siderite (SI) cementation. Chlorite is absent in TST sandstones but was found frequently in LST-HST sandstones. Early kaolinite is not present in LST sandstones but occurred frequently in LST-HST sandstones.*

*The distribution of mesogenetic cements relative to sequence stratigraphy is different in the U and T units. In the U sandstones, calcite is frequent in LST deposits and absent in the LST-HST. Fe-dolomite/ankerite is abundant only in the TST. S2 siderite is present in the TST and LST, but absent in the LST-HST. Quartz cement and kaolinite/dickite are equally distributed in all systems tracts. In the T sandstones Fe-dolomite/ankerite is only abundant in the TST, whilst calcite, quartz and dickite have similar distributions in all the systems tracts.*

*The distribution of kaolinite cement is interpreted to be the result of relatively more intense meteoric-water flux occurring during sea-level fall, whereas chlorite cement may have formed through burial diagenetic transformation of precursor clays e.g. berthierine which was precipitated in mixed marine-meteoric waters in tidal channel and estuarine environments.*

*Chlorite cement in the T and U sandstones appears to have retarded development of quartz overgrowths, and 12–13% primary porosity is retained. The T sandstones (LST-HST) contain up to 4% chlorite cement. Little evidence for chemical compaction was found with the exception of occasional concave-convex grain contacts.*

*Eogenetic siderite appears to have helped to preserve reservoir quality through supporting the sandstone framework against further compaction, but mesogenetic calcite*

<sup>1</sup> Facultad de Ciencias del Mar y Ambientales, Dpto. de Ciencias de la Tierra UCA, 11510 Cádiz, Spain.

\*Author for correspondence, e-mail:  
jenny.estupinan@uca.es

<sup>2</sup> Dpto. de Petrología y Geoquímica, Facultad de Geología, UCM, 28040 Madrid, Spain.

<sup>3</sup> GG Consulting, Dorsten, Barkenberger Allee 150A, 46286, Germany.

<sup>4</sup> Dpt. de Geoquímica, Petrología i Prospecció Geològica, Universitat de Barcelona, 08028 Barcelona, Spain.

**Key words:** Sandstone diagenesis, sequence stratigraphy, reservoir quality, Napo Formation, Oriente Basin, Ecuador.

*has considerably reduced primary porosity. Eogenetic siderite (S1) was partly replaced by later carbonate cements such as late siderite (S2) and Fe-dolomite. Although there appears to be a relationship in the Napo Formation between the occurrence of siderite S1 and sequence stratigraphy, the relationship may change when original volumes of siderite are considered. There is likewise partial replacement of early kaolinite and recrystallization to dickite which masks the amount of original early kaolinite. Since the amount of early kaolinite could not be confirmed, the relationship to sequence stratigraphy is tentative. Only chlorite seems to have a clear relationship to sequence stratigraphic framework in the Napo Formation.*

*The high intergranular volume (IGV) of the sandstones indicates that cementation played a more important role than mechanical and chemical compaction in both Napo Formation sandstone members. Later dissolution of feldspar grains and siderite cements was the main process of secondary porosity development (up to 11% in the U sandstones).*

## INTRODUCTION

The development of porosity within deeply buried sandstones is a subject of considerable debate. Many authors have suggested that the removal of either framework grains or intergranular cements is the dominant process of porosity generation at depth in hydrocarbon reservoirs (Hayes, 1979; Schmidt and McDonald, 1979; Burley and Kantorowicz, 1986). A number of recent papers have demonstrated that early diagenetic alterations in sandstones, which are important for reservoir preservation during progressive burial, can be better constrained when linked to a sequence stratigraphic framework (Morad *et al.*, 2000; Ketzer *et al.*, 2003a; Ketzer *et al.*, 2003b). These authors have suggested that the spatial distribution of eogenetic alterations in fluvial, transitional and marine sediments is strongly influenced by sea level changes and depositional facies. Changes in relative sea level allow the delineation of reservoir quality as well as the spatial and temporal distribution of sandstones and carbonates in a sequence stratigraphic context (Van Wagoner *et al.*, 1990; Posamentier and Allen, 1999). Sandstones adjacent to parasequence boundaries are, for instance, commonly cemented by carbonates because of the prolonged residence time of the sediments close to the sediment-water interface (Van Wagoner *et al.*, 1990; Posamentier and Allen, 1999). Changes in pore-water chemistry promote diagenetic alterations such as the dissolution of framework grains and the formation of kaolinite (Curtis, 1967, 1987; Coleman and Raiswell, 1993). The reservoir quality of

sandstones below sequence boundaries can be improved as a result of the percolation of meteoric waters and the dissolution of unstable framework grains and cements. This may also apply to sandstones below major unconformities where leaching has commonly been observed (Van Wagoner *et al.*, 1990; Posamentier and Allen, 1999).

Attempts have been made to link the distribution of clay minerals to the sequence stratigraphy framework of clastic deposits (Ketzer *et al.*, 2003b). The authigenesis of clay minerals appears to be mainly related to parasequence boundaries and especially to maximum flooding surfaces. Permeable sandstones below subaerially-exposed sequence boundaries are subjected to mechanical infiltration by clays in semi-arid climates, or to pervasive kaolinitization due to percolation of undersaturated meteoric water in humid climatic conditions (Morad *et al.*, 2000; El-Ghali *et al.*, 2006).

This study focuses on the spatial and temporal distribution of diagenetic processes in the Cretaceous Napo Formation sandstones and their relationship with depositional facies and sequence stratigraphy. The study makes use of previously published sequence stratigraphic surfaces and systems tract definitions (Table 1) as well as detailed core descriptions (Ramirez *et al.*, 1995; White *et al.*, 1997).

Diagenetic regimes used in this paper follow Morad *et al.* (2000) and are: (a) eodiagenesis, with temperatures <70°C, during which pore water chemistry is controlled by surface waters; and (b) mesodiagenesis (burial diagenesis), which is controlled by pore fluids under increased pressure and temperature.

## GEOLOGICAL SETTING

The Oriente Basin covers parts of Colombia, Ecuador, Peru, Bolivia and Brazil (Fig. 1). The present-day morphology of the basin results from Late Cretaceous transgression followed by subduction-induced uplift of the Cordillera Real Mountains and formation of the back-arc basin to the east (Fig. 1). Compressional events occurred in the Early Cretaceous and Turonian resulting in inversion of the Permo-Triassic and Jurassic sequences throughout the basin. Structural traps developed during the Turonian inversion phase (Baldock, 1982; Dashwood and Abbotts, 1990).

The reservoir units studied belong to the Napo U and T sandstone members (Upper Albian - Upper Cenomanian: Fig. 2), which are composed of cyclic sequences of limestones, shales and sandstones deposited on a low-energy shallow-marine platform. These cycles were controlled by changes in relative sea level (White *et al.*, 1995). Two depositional stages are proposed for the U and T intervals:

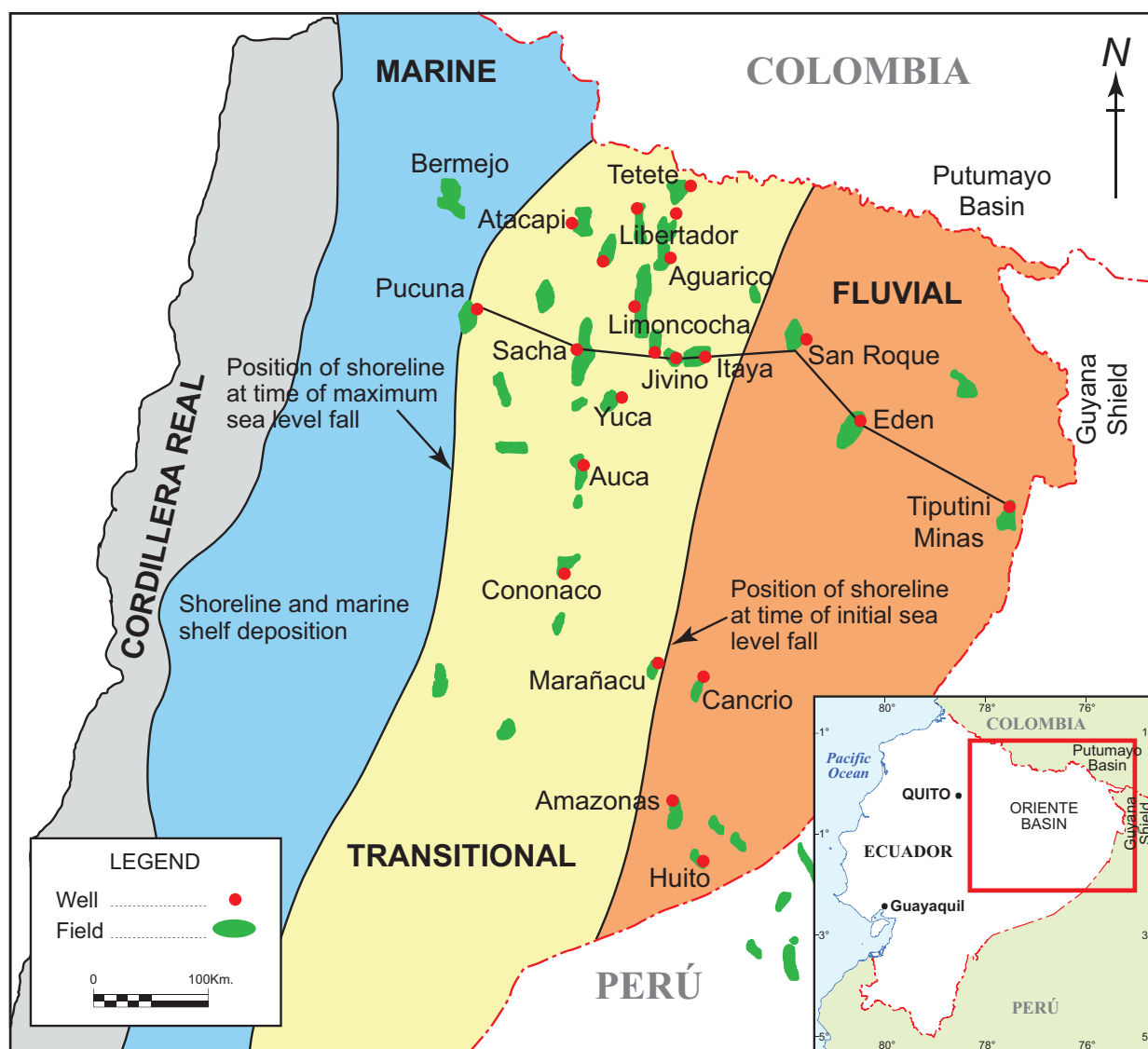


**Fig. 1.** Location map of the Oriente Basin, Ecuador, and palaeogeographic map of the Napo Formation showing the shoreline position at the times of initial and maximum sea level fall (adapted from White *et al.*, 1995). Sampled wells are indicated by dots. Profile marks the cross-section in Fig. 4.

**Table 1.** Definition of sequence stratigraphic terms used in this study (after Posamentier and James, 1993; Zaitlin *et al.*, 1994).

|  | Abbreviation | Definition   |
|--|--------------|--|
| Lowstand systems tract                                       | LST          | Sediment deposited in incised valleys with estuarine influence during relative sea level lowstand and initial rise |
| Transgressive system tract                                   | TST          | Shallow marine sediments deposited over incised valleys during transgression                                       |
| Highstand systems tract                                      | HST          | Sediments deposited during relative sea level highstand  |
| Maximum flooding surface                                     | MFS          | Surface located at the base of the HST, sediments deposited during maximum relative sea level                      |
| Sequence boundary  | SB           | Erosional unconformity at the inner shelf located at the base of the LST   |
| Lowstand systems tract influenced by Highstand systems tract | LST-HST      | Transitional environments: Sediment deposited in tidal channels and estuarine settings                             |

| AGE                  | FORM.                           | LITHOL. | THICK. APROX. (m) | REMARKS  |
|----------------------|---------------------------------|---------|-------------------|--|
| CURRENT              | ALLUVIAL                        |         |                   |  |
| PLEIST.              | TERRACE                         |         |                   |  |
| PLIO. to MIOCENE     | CHAMBIRA<br>ARAJUNO<br>CHALCANA |         | 1500 to 2900      | Continental sediments  |
| OLIGOC.              | ORTEGUAZA                       |         | 31-3040           | Shallow to marine  |
| OLIGOC. TO EOCENE    | TIYUYACU                        |         | 150-640           | Continental sediments. Shales and conglomerates. Local production              |
| PALEOC. TO U. CRET.  | TENA                            |         | 28-760            | Continental to shallow marine, shale. Some production                          |
| UPPER TO LOWER CRET. | NAPO                            |         | 213-762           | Marine shales, limestone and sandstone. Frequent oil production (U and T sand) |
| LOWER CRET.          | HOLLIN                          |         | 213-914           | Continental reservoir  |
|                      | CHAPIZA                         |         | 0-244             | Volcanics and shales, continental mudstones and sandstone                      |
| JURASSIC             | SANTIAGO                        |         | 1500              | Marine limestone and sandstone   |
| PERMIAN PENNSYL      | MACUMA                          |         | >700              | Limestone, sandstone and shale   |
| MISSISS. AND OLDER   | PUMBUIZA                        |         | ??                | Marine shale with sandstone and limestone locally metamorphosed                |

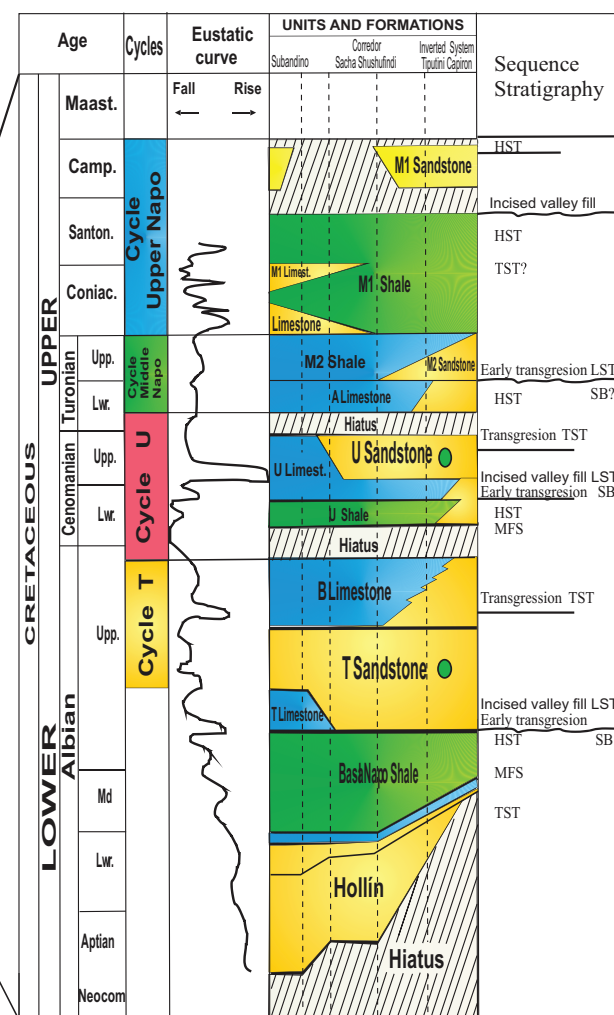


Fig. 2. Generalised stratigraphic column for the Oriente Basin with lithostratigraphic nomenclature (modified from Almeida, 1986). Column to right shows reservoirs in the U and T sandstones of the Napo Formation (Christophoul and Rivadeneira, 1986, modified from Jaillard, 1997).

Depositional stage 1 (T sandstone interval): Sea level fall during the Late Albian (ca. 98 Ma) created a major sequence boundary and an erosive drainage network subsequently filled by incised valley sandstones during early transgressive sea-level rise; and

Depositional stage 2 (U sandstone interval): A later sea level fall during the middle Cenomanian (ca. 94 Ma) resulted in another erosional sequence boundary. The U sandstone represents the subsequent incised valley fill deposited during early transgression (White *et al.*, 1995).

Although similar in terms of environment of deposition, the sandstone members differ in composition and maturity.

## MATERIALS AND METHODS

Fifty-four core samples from the Napo Formation were selected from 22 wells at depths of 4787 ft to 10,250 ft. Additional data from 59 wells was obtained from Occidental and Oryx Ecuador, and from internal reports concerning sedimentary environment, stratigraphic sequences and petrography.

After removing any oil present with dichloromethane, the samples were impregnated with blue-stained resin prior to thin sectioning. Thin sections were stained with sodium cobaltinitrite and with Alizarin Red-S and potassium ferricyanide (for K-feldspar and for carbonates, respectively).

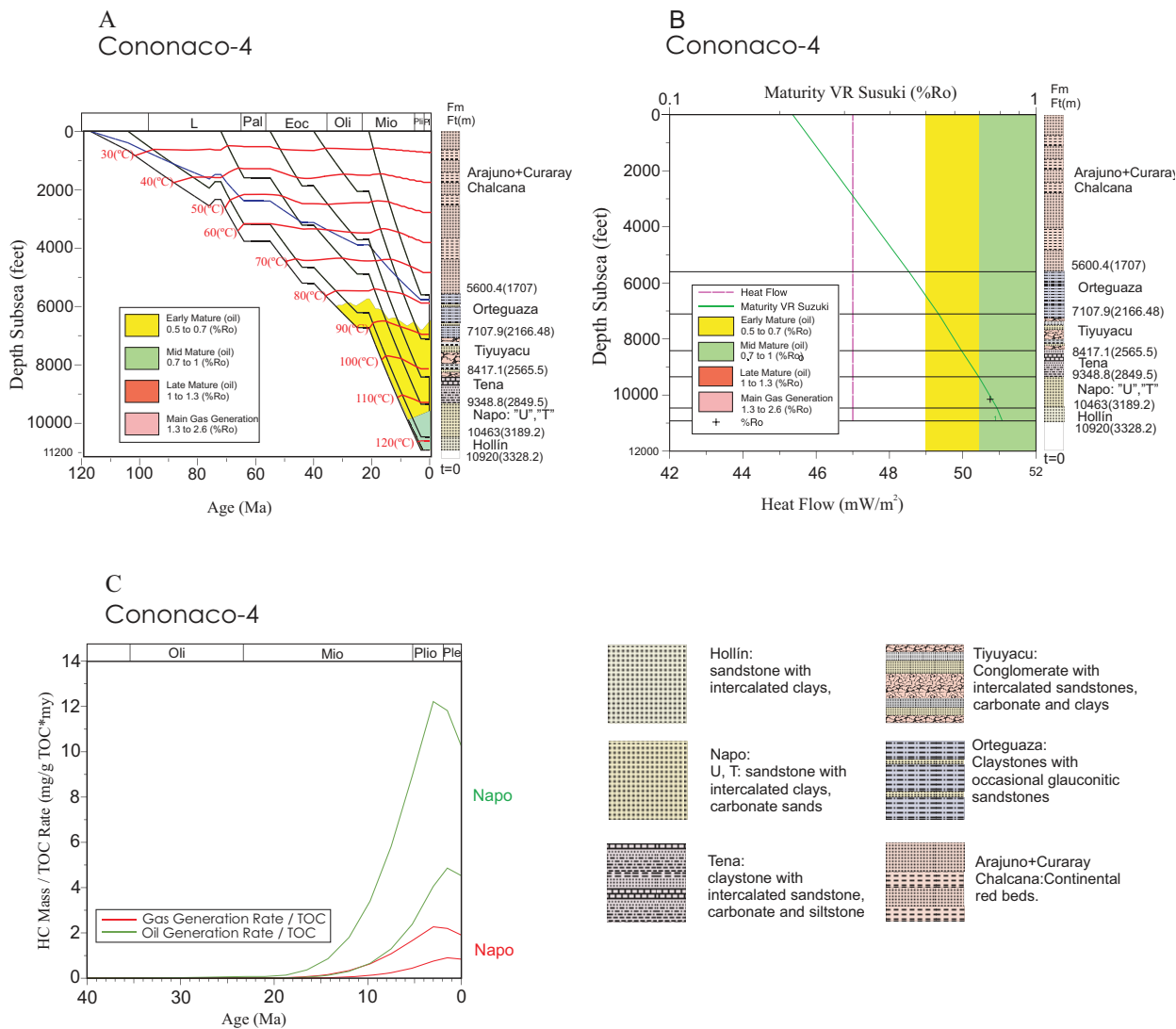


**Fig. 3. (A) Burial and thermal history of the Napo Formation in well Cononaco-4, Oriente Basin (see location in Fig. 1) (after Estupiñan, 2006); (B) Plot of heat flow versus depth; (C) Profiles of oil and gas generation history.**

Quantification of the framework composition was performed by counting 300 points per thin section. Cathodoluminescence (CL) was applied using a “cold” *Technosyn 8200 Mk 4* apparatus. Bulk mineralogy was confirmed by X-ray diffraction, employing a *Philips PW 1720* diffractometer equipped with Cu ( $K\alpha$ ) radiation. The sequence of diagenetic minerals was studied using a scanning electron microscope (SEM) model *JEOL JSM 6400* equipped with an energy-dispersive X-ray microanalyzer in secondary electron and backscattered electron modes (BSE). The chemical compositions were determined by microprobe analyses using a *JEOL JXA-8900* model. Detection limits are approximately 100 ppm for Mg, 250 ppm for Mn and 300 ppm for Fe. The BSE system of the microprobe was used for detecting zonation in cements.

Stable carbon and oxygen isotope analyses were performed on thirteen representative carbonate-

cemented sandstone samples. Samples containing more than one phase of cement were separated by chemical sequential methods (Al-Aasm *et al.*, 1990). Isotope values are in ‰ and refer to the V-PDB standard.

Fluid inclusion microthermometry was performed on quartz cements from three representative samples using a *Linkam THMSG 600* heating-cooling stage. The system was calibrated at a low temperature by the inclusion of pure  $\text{CO}_2$  in topaz (-56.6°C) and synthetic inclusions of pure water in quartz (0.015°C), and at a high temperature by standard melting temperatures provided by Merck.

## BURIAL AND THERMAL EVOLUTION

Since burial temperature and hydrocarbon migration have an impact on diagenesis, the burial history of the sediments (c.f. Posamentier and Allen, 1999) and

the source rock maturation history was also studied in previous investigations.

Sediments were buried to a maximum depth of 4920 ft in the eastern part of the basin and to 10,470 ft in the centre. The burial and thermal histories, based on data from well *Cononaco-4* (Fig. 3A), were modelled using *BasinMod 1-D* to estimate the timing of hydrocarbon generation, expulsion, and migration (Estupiñán, 2006). The burial history was reconstructed based on well data. Uncorrected and therefore underestimated BHTs of 78 to 112 °C are reported for *Cononaco-4*. An equivalent vitrinite reflectance is 0.75% Ro. Heat flow values typical for back-arc basins ( $51\text{mW/m}^2$ ) were estimated from the modelling (Fig. 3B). The burial history plot based on the *Cononaco-4* data suggests that the oil window was reached for the Napo level at approximately 120°C in the Miocene (8 Ma) at a burial depth of 9370 ft (Fig. 3C). The actual formation temperatures were probably close to 120 °C, as estimated by the *BasinMod* modelling.

## SEQUENCES AND SYSTEMS TRACTS

The Napo Formation in the Oriente Basin comprises a succession of marine claystones, limestones and sandstones, which correspond to transgressive and regressive cycles (Fig. 2) (White *et al.*, 1995). The formation was deposited on a stable marine shelf. Claystone-limestone units represent transgressive systems tract (TST) deposits. The sandstones represent lowstand systems tracts (LST), and involve westward progradation of littoral to fluvio-deltaic facies belts.

The Napo T member comprises a sequence of stacked sandstones with interbedded siltstones and carbonaceous claystones (Fig. 4). The Napo U member has some similarities with the T member, the lower part being more arenaceous and the upper part more argillaceous. At the base, the U interval shows a reduction in sandstone from east to west (cross-section Fig. 4) demonstrating sea level control on the facies association.

Interpretations of the depositional environments of the U and T sandstones are based on core samples and logs. The sequence boundaries at the bases of the U and T sandstones are erosional events forming incised valleys associated with falls of relative sea level. (Ramirez *et al.*, 1995; White *et al.*, 1997; Barragan *et al.*, 2004).

In the following section, the stratigraphy of the Napo T and U sandstone members are described in more detail.

### Napo T

The Napo T member can be divided into Basal T, Main T and Upper T intervals.

The Basal T interval comprises marine shelf mudstones, glauconitic shoals, shoreline sands and coastal plain sandstones (White *et al.*, 1997; Barragan *et al.*, 2004). At the top of the Basal T are marine shelf mudstones and glauconitic shoal facies in the western and central parts of the Oriente Basin, and shoreline and coastal plain facies in the east.

The Basal T is overlain directly by the Main T, and the contact is considered to be a sequence boundary (SB) (Fig. 4) (White *et al.*, 1997). Following highstand deposition of the Basal T shales, this boundary represents an erosional surface caused by subsequent sea level fall. A rise in sea-level followed the incised valley deposition of the Main T interval. Main T deposits are interpreted to be of shoreline and fluvial origin, contrasting with the marine-influenced deposits in the Basal T (Fig. 4). The top of the Main T consists of tidal shoal, deltaic and tidal-channel sandstones with clay laminations/drapes.

The overlying Upper T consists of lagoonal facies passing up to marine facies. The latter consist of glauconitic sandstones, calcareous sandstones and shales. These are overlain by the Napo B limestone. The glauconitic sandstones and the Napo B limestone are interpreted to form a highstand systems tract (Fig. 4) (White *et al.*, 1997; Barragan *et al.*, 2004).

During Napo T deposition, sea level rise and fall created a succession of basin-wide shoreline shifts across the low gradient shelf of the Oriente continental margin. The Basal T comprises sedimentation during a sea level highstand. At the highest point, the shoreline was located in the central part of the Oriente Basin and low-energy coastal plain sediments were deposited with tide influenced shoreline and offshore marine shoal strata (Barragan *et al.*, 2004). At the end of the Basal T, a fall in sea level shifted the shoreline westwards into the western Oriente Basin, exposing the previous depositional surface as a sequence boundary (Fig. 4). The resulting fluvial incision created a network of incised valleys. These valleys were filled by the Main T sandstones when sea level began to rise again. Further sea level rise created a basin-wide shoreline to marine parasequence comprising the Upper T (Fig. 4) (Barragan *et al.*, 2004, Ramirez *et al.*, 1995).

### Napo U

The Napo U member, which consists of sandstones, mudstones and fossiliferous limestones, is divided into the Main U and Upper U intervals.

A relative sea level fall during the middle Cenomanian (94 Ma) is interpreted to be responsible for the presence of the sequence boundary at the base of the Main U (Fig. 4) (Ramirez *et al.*, 1995). The Main U consists of cross-bedded sandstones and wavy-bedded sandy siltstones. The unit was

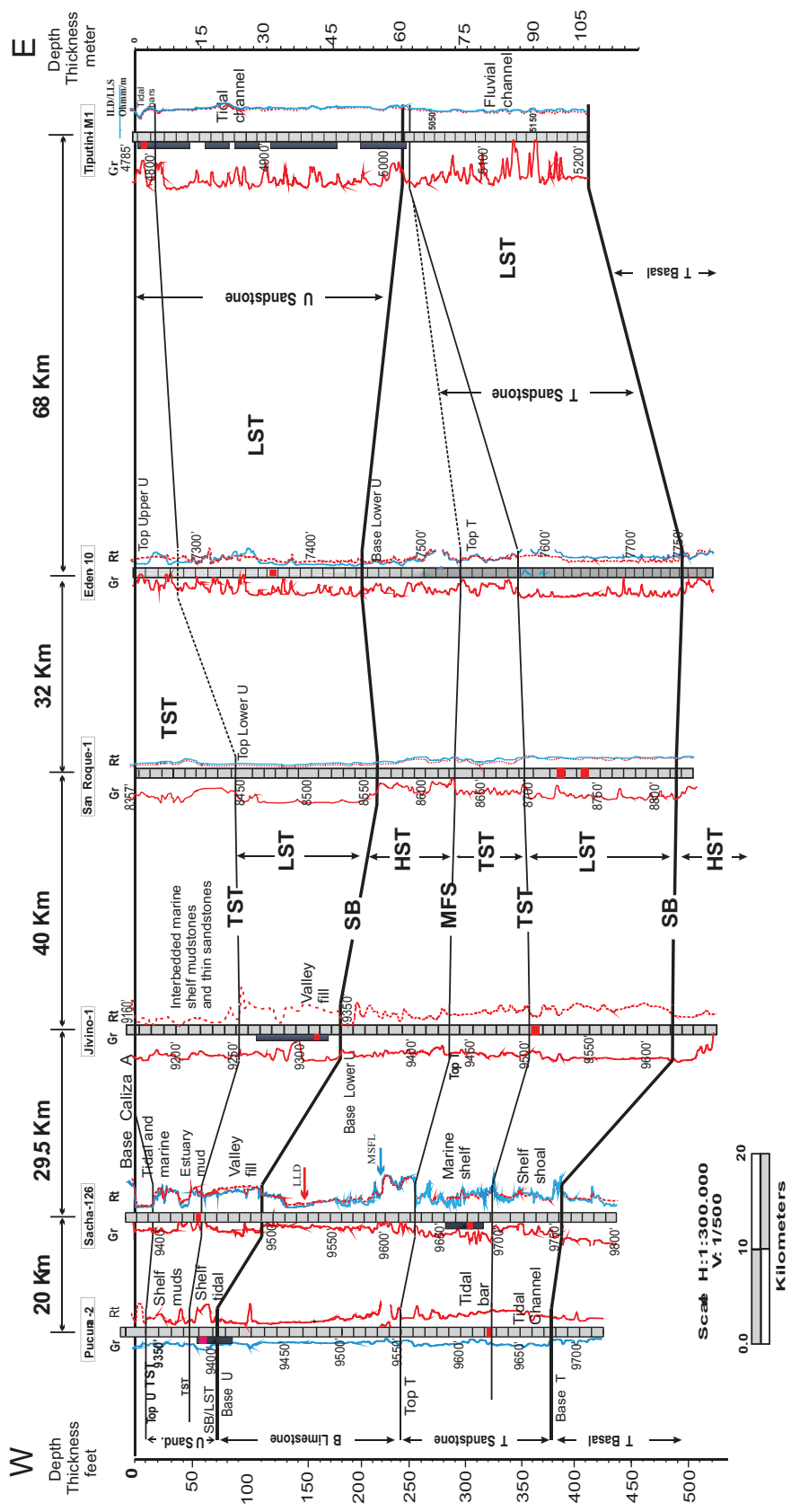
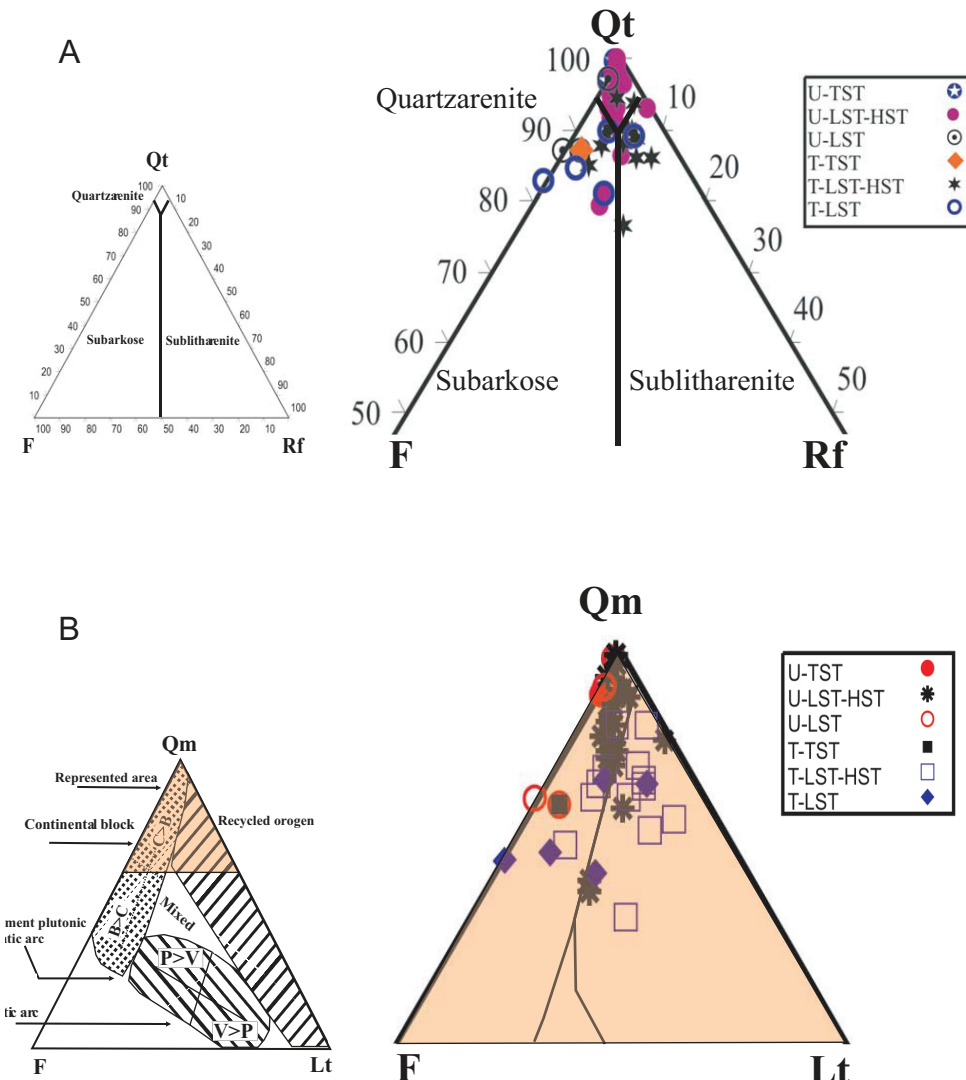


Fig. 4. Stratigraphic cross-section of the Napo Formation, showing correlation between six wells in the Oriente Basin with sequence stratigraphic interpretation. See cross-section location in Fig. 1. I. HST: highstand systems tract; LST: transgressive systems tract; TST: transgressive surface; TS: transgressive surface boundary.



**Fig. 5.**Ternary plots showing the detrital composition and provenance of representative sandstones from the Napo Formation. (A) Qt-F-RF diagram (Dott, 1964 and modified by Pettijohn et al., 1972). Qt = Quartz, F= Feldspar, RF = Rock fragments. (B) Restored ternary diagram Qm-F-Lt (Dickinson, 1985). Qm (monocrystalline quartz), -F (K-feldspar + plagioclase), -Lt (rock fragments + polycrystalline quartz + chert) indicating potential source areas. Based on diagram from Dickinson and Suczek (1979), which considers polycrystalline quartz with crystals exceeding 0.0625mm as simple monocrystalline crystals. As a result, the sandstone samples plot in the “continental blocks” field, and some of the T sandstones plot in the “recycled orogen” field.

deposited during early sea level rise; incised valleys were widened and transformed into estuaries in which tidally influenced fluvial sandstones were deposited. The top of the U interval is composed of glauconitic sandstones with interbedded mudstone lenses belonging to a HST and marks the end of the transgressive phase.

#### SANDSTONE PETROGRAPHY

The Napo T sandstones are subarkoses with an average composition of  $Qt_{90}F_7RF_3$ . Napo U sandstones are quartzarenites with a fairly uniform composition of  $Qt_{96}F_3RF_1$  with minor subarkoses (Fig. 5A; Tables 2 and 3). Both sandstones are fine- to coarse-grained;

grains are rounded to subrounded with moderate to good sorting. Minor clay matrix (pseudomatrix and epimatrix), derived from mechanical deformation and alteration of the metamorphic rock fragments, glauconite and feldspars, occurs in all sandstone samples (< 1%). Quartz grains are monocrystalline with frequent corrosion cavities (pits) (Fig. 6A). Few polycrystalline grains are present (Fig. 6B). Chert grains are rare. K-feldspar is more abundant than plagioclase in all depositional facies, varying between 0 and 7 %. Feldspars are occasionally albited (Fig. 6C). Most feldspar grains show evidence of dissolution. Biotite and muscovite (av. 0-2%) are frequently kaolinitised (Fig. 6D). Rock fragments are volcanic, metamorphic (quartzite) and sedimentary

**Table 2. Representative modal analyses of the U sandstones of the Napo Formation, Oriente Basin, Ecuador.**

|                      | TST                       |       |       |            |                 |              | LST-HST     |                       |                    |                    |                    |                       | LST                 |                 |               |                |              |                |
|----------------------|---------------------------|-------|-------|------------|-----------------|--------------|-------------|-----------------------|--------------------|--------------------|--------------------|-----------------------|---------------------|-----------------|---------------|----------------|--------------|----------------|
|                      | U sandstone<br>depth (ft) | PC-2  | TT-1  | Av.<br>n=2 | AA-10<br>9192.5 | AT-2<br>9402 | CN4<br>9988 | IY-B6 p<br>Av.<br>n=7 | JV-1<br>Av.<br>n=4 | JV-3<br>Av.<br>n=2 | LM-9<br>Av.<br>n=4 | SC-126<br>Av.<br>n=19 | YC-2<br>Av.<br>n=19 | Average<br>n=19 | ED-10<br>7365 | MR-1<br>8958.2 | TM-1<br>4787 | Average<br>n=3 |
| Qmr                  | 32.6                      | 40.0  | 36.3  | 31.8       | 44.3            | 34.6         | 39.6        | 38.0                  | 38.2               | 38.6               | 36.0               | 34.3                  | 37.5                | 35.3            | 36.7          | 40.7           | 37.6         | 35.9           |
| Qmo                  | 6.7                       | 7.5   | 7.1   | 5.3        | 6.7             | 10.0         | 8.0         | 14.0                  | 10.2               | 9.3                | 7.0                | 12.4                  | 9.0                 | 11.0            | 10.0          | 4.7            | 8.6          | 8.1            |
| Qp2-3                | 6.0                       | 10.7  | 8.3   | 11.3       | 6.7             | 8.3          | 5.0         | 3.8                   | 7.4                | 7.0                | 4.4                | 9.7                   | 7.4                 | 5.0             | 4.7           | 3.3            | 4.3          | 5.9            |
| Qp >3                | 1.7                       | 1.3   | 1.5   | 3.0        | 2.0             | 2.7          | 1.0         | 1.8                   | 2.6                | 0.3                | 1.0                | 3.7                   | 1.9                 | 2.0             | 0.9           | 1.0            | 1.3          | 1.6            |
| Q in Fr              | 0.0                       | 0.0   | 0.0   | 0.0        | 0.0             | 0.0          | 0.3         | 0.2                   | 0.3                | 0.3                | 0.3                | 0.0                   | 0.1                 | 0.3             | 0.0           | 0.3            | 0.2          | 0.1            |
| K-F                  | 0.7                       | 0.3   | 0.5   | 0.7        | 1.3             | 1.0          | 2.0         | 2.0                   | 0.5                | 0.7                | 2.3                | 0.0                   | 1.1                 | 6.7             | 0.0           | 2.3            | 3.0          | 1.6            |
| CC3 replace KF       | 0.7                       | 0.0   | 0.3   | 1.3        | 0.0             | 1.3          | 0.2         | 0.0                   | 0.0                | 0.0                | 0.0                | 0.0                   | 0.3                 | 0.0             | 0.7           | 3.7            | 1.4          | 0.8            |
| Ptg + Alb            | 0.0                       | 0.0   | 0.0   | 0.0        | 0.3             | 0.7          | 0.8         | 0.3                   | 0.1                | 0.0                | 1.4                | 0.7                   | 0.4                 | 0.0             | 0.7           | 1.4            | 0.7          | 0.4            |
| Chert                | 0.0                       | 0.0   | 0.0   | 0.0        | 0.0             | 0.0          | 0.3         | 0.0                   | 0.1                | 0.3                | 0.0                | 0.0                   | 0.1                 | 0.0             | 0.0           | 0.0            | 0.0          | 0.0            |
| Opques               | 0.3                       | 0.0   | 0.2   | 0.0        | 0.7             | 0.0          | 0.0         | 0.8                   | 1.6                | 0.7                | 4.3                | 0.0                   | 0.8                 | 0.0             | 0.0           | 0.0            | 0.0          | 0.4            |
| Muscovite            | 0.0                       | 0.0   | 0.0   | 1.0        | 0.0             | 0.3          | 0.3         | 0.2                   | 0.0                | 0.0                | 0.0                | 1.0                   | 0.3                 | 1.0             | 0.0           | 0.0            | 0.3          | 0.2            |
| Biotite              | 0.0                       | 0.0   | 0.0   | 0.0        | 0.0             | 0.0          | 0.3         | 0.0                   | 0.0                | 0.3                | 0.0                | 0.0                   | 0.1                 | 0.0             | 0.0           | 0.0            | 0.0          | 0.0            |
| Heavy minerals       | 0.0                       | 0.1   | 0.1   | 0.2        | 0.0             | 0.0          | 0.0         | 0.1                   | 0.0                | 0.0                | 0.0                | 0.1                   | 0.1                 | 0.6             | 0.3           | 0.3            | 0.1          | 0.1            |
| Total                | 48.6                      | 59.9  | 54.3  | 54.7       | 61.9            | 58.9         | 57.8        | 61.3                  | 60.9               | 57.5               | 56.7               | 61.9                  | 59.2                | 61.9            | 53.9          | 57.4           | 57.8         | 55.2           |
| Q. overgrowth        | 12.0                      | 14.0  | 13.0  | 15.0       | 18.1            | 10.0         | 15.0        | 14.0                  | 16.0               | 17.0               | 7.0                | 9.0                   | 13.5                | 11.0            | 10.0          | 12.0           | 11.0         | 12.2           |
| Calcite              | 2.0                       | 0.0   | 1.0   | 0.0        | 1.0             | 0.2          | 0.0         | 0.3                   | 0.0                | 0.0                | 0.0                | 0.2                   | 0.0                 | 0.0             | 21.0          | 1.0            | 7.3          | 3.2            |
| Fe-dolomite/ankerite | 10.7                      | 0.0   | 5.3   | 2.0        | 0.0             | 0.0          | 0.0         | 0.0                   | 0.0                | 14.7               | 0.0                | 1.7                   | 0.0                 | 0.0             | 1.7           | 0.6            | 4.3          |                |
| Siderite             | 2.4                       | 0.7   | 1.5   | 0.0        | 0.0             | 0.0          | 0.0         | 0.0                   | 0.4                | 0.0                | 0.0                | 0.1                   | 0.0                 | 0.0             | 3.0           | 1.0            | 1.2          |                |
| Kaolin               | 0.0                       | 4.0   | 2.0   | 3.3        | 3.7             | 2.0          | 2.8         | 3.0                   | 5.0                | 6.7                | 1.3                | 3.0                   | 3.5                 | 2.1             | 0.0           | 0.3            | 0.8          | 1.4            |
| Pyrite               | 0.7                       | 0.0   | 0.3   | 0.7        | 0.0             | 0.7          | 0.3         | 0.8                   | 0.0                | 0.0                | 0.0                | 0.2                   | 0.0                 | 0.2             | 2.3           | 0.0            | 0.8          | 0.6            |
| Chlorite             | 0.0                       | 0.0   | 0.0   | 2.7        | 0.0             | 1.0          | 0.0         | 1.0                   | 0.0                | 0.0                | 0.0                | 0.7                   | 0.5                 | 1.0             | 0.0           | 0.0            | 0.3          | 0.3            |
| Total cement         | 27.7                      | 18.7  | 23.2  | 21.8       | 14.7            | 18.3         | 18.8        | 21.3                  | 24.1               | 23.0               | 12.7               | 19.7                  | 14.1                | 33.3            | 18.0          | 21.8           | 23.1         |                |
| Epimatrix            | 3.3                       | 4.0   | 3.7   | 7.0        | 2.3             | 6.3          | 2.8         | 0.2                   | 0.4                | 2.0                | 2.0                | 6.0                   | 3.3                 | 1.7             | 0.3           | 1.3            | 1.1          | 2.6            |
| Pseudomatrix         | 0.0                       | 0.0   | 0.0   | 1.0        | 0.0             | 1.0          | 0.0         | 1.0                   | 0.3                | 0.3                | 1.6                | 0.5                   | 0.7                 | 0.0             | 0.0           | 0.2            | 0.3          |                |
| Total                | 3.3                       | 4.0   | 3.7   | 8.0        | 2.3             | 7.3          | 2.8         | 1.2                   | 0.7                | 2.3                | 2.3                | 7.6                   | 3.8                 | 2.4             | 0.3           | 1.3            | 1.3          | 2.8            |
| Glauconite           | 5.7                       | 0.0   | 2.9   | 1.0        | 0.6             | 0.1          | 0.0         | 0.2                   | 0.0                | 0.0                | 0.3                | 0.1                   | 0.2                 | 0.3             | 5.7           | 0.0            | 2.0          | 2.6            |
| P1 porosity          | 9.0                       | 13.4  | 11.2  | 5.7        | 8.3             | 11.7         | 13.1        | 10.6                  | 14.3               | 14.4               | 16.0               | 7.0                   | 11.5                | 13.3            | 4.7           | 13.3           | 10.4         | 10.3           |
| P2 porosity          | 5.7                       | 4.0   | 4.9   | 7.0        | 5.1             | 7.3          | 7.9         | 7.9                   | 2.8                | 1.7                | 1.7                | 10.7                  | 5.6                 | 8.0             | 2.0           | 10.0           | 6.7          | 6.0            |
| Total Porosity       | 14.7                      | 17.4  | 16.1  | 12.7       | 13.4            | 19.0         | 21.0        | 18.5                  | 17.2               | 16.1               | 17.7               | 17.7                  | 21.3                | 6.7             | 23.3          | 17.1           | 16.3         |                |
| Grain size           | Fu - Fl                   | fl-ml | Fu-mu | fl-ml      | Fu-mu           | fl-ml        | Fu-mu       | fl-fu                 | fl-fu              | fl-fu              | fl-fu              | fl-fu                 | fl-fu               | fl-fu           | fl-fu         | fl-fu          | fl-fu        |                |
| Sorting              | good                      | good  | Mod.  | good       | mod             | good         | good        | good                  | good               | mod                | mod                | mod                   | mod                 | mod             | good          | good           | mod.         |                |
| IGV                  | 36.8                      | 33.7  | 35.3  | 38.0       | 35.8            | 32.3         | 35.5        | 34.8                  | 37.2               | 38.4               | 37.7               | 28.0                  | 35.1                | 31.3            | 39.7          | 36.3           | 35.8         | 35.9           |

n = number samples analyzed in the well

**Table 3.** Representative modal analyses of the Napo Formation, Oriente Basin, Ecuador.

| T sandstone depth (ft) | TST     |         |         |         |         | LST - HST |         |         |         |         |         |         |         |         |         | LST       |           |           |         |         |      |            |            |   |  |
|------------------------|---------|---------|---------|---------|---------|-----------|---------|---------|---------|---------|---------|---------|---------|---------|---------|-----------|-----------|-----------|---------|---------|------|------------|------------|---|--|
|                        | PC-2    | AA-10   | AC-16   | CN-4    | CN-4    | IT-B-6    | JV-1    | JV-3    | LM-9    | SC-99   | SC-105  | SC-126  | YC-2    | YB-1    | Av.     | AZ-1      | CR-1      | ED-10     | HT-1    | S RQ-1  | Av.  | Average    | Total n=29 | % |  |
| n=3                    | Av.     | 9412    | 9976    | 10248   | 10249   | Av.       | 9500    | 9492    | 9699    | 9649    | 9757    | 9670    | 9791    | 9829    | n=17    | 9663      | 8863      | Av.       | 9488    | n=2     | n=9  | Total n=29 | %          |   |  |
| %                      | %       | %       | %       | %       | %       | n=5       | %       | %       | %       | %       | %       | %       | %       | %       | %       | %         | %         | %         | %       | %       | %    | %          | %          | % |  |
| Qmr                    | 36.0    | 27.7    | 32.3    | 31.9    | 22.0    | 38.1      | 32.0    | 26.7    | 35.0    | 33.6    | 32.4    | 31.4    | 37.0    | 31.7    | 27.2    | 23.0      | 30.0      | 29.0      | 34.6    | 28.8    | 32.2 |            |            |   |  |
| Qmo                    | 3.0     | 10.3    | 10.0    | 5.0     | 6.3     | 6.6       | 11.0    | 3.0     | 5.0     | 7.4     | 6.7     | 6.1     | 8.2     | 6.9     | 4.7     | 10.0      | 6.0       | 6.0       | 4.3     | 6.2     | 5.4  |            |            |   |  |
| Qp2-3                  | 6.0     | 10.0    | 6.3     | 5.7     | 2.3     | 8.0       | 7.0     | 5.3     | 4.3     | 5.3     | 5.0     | 8.3     | 3.0     | 2.4     | 5.6     | 3.7       | 5.7       | 5.0       | 3.3     | 6.7     | 4.9  | 5.5        |            |   |  |
| Qp>3                   | 0.7     | 1.7     | 1.3     | 0.7     | 0.7     | 1.6       | 1.0     | 3.0     | 2.0     | 1.7     | 0.3     | 1.4     | 1.7     | 1.4     | 1.3     | 3.0       | 3.0       | 2.0       | 1.0     | 2.1     | 1.4  |            |            |   |  |
| Q ffr.net              | 1.0     | 1.0     | 0.0     | 0.7     | 0.7     | 0.0       | 0.0     | 1.0     | 0.7     | 0.3     | 0.0     | 0.0     | 0.0     | 0.0     | 0.4     | 0.3       | 0.3       | 0.3       | 0.7     | 0.2     | 0.4  | 0.6        |            |   |  |
| K-F                    | 1.0     | 0.0     | 0.0     | 0.0     | 0.0     | 1.0       | 0.3     | 5.0     | 1.0     | 0.0     | 0.0     | 0.0     | 0.0     | 0.0     | 1.0     | 0.7       | 1.2       | 1.4       | 3.0     | 1.7     | 0.0  | 1.5        | 1.0        |   |  |
| CO3-KF                 | 2.6     | 0.0     | 0.0     | 0.0     | 0.0     | 0.0       | 0.0     | 0.0     | 1.0     | 0.0     | 0.0     | 0.0     | 0.0     | 0.0     | 0.1     | 0.0       | 0.0       | 0.0       | 0.0     | 2.3     | 0.0  | 0.5        | 1.1        |   |  |
| Ptg+Alb.               | 2.0     | 3.0     | 4.0     | 4.6     | 0.7     | 3.0       | 0.0     | 1.7     | 1.7     | 0.6     | 2.6     | 1.0     | 2.0     | 4.0     | 4.9     | 0.1       | 4.5       | 1.8       | 3.1     | 2.4     |      |            |            |   |  |
| Opaques                | 1.3     | 3.2     | 3.0     | 1.0     | 2.0     | 1.8       | 1.0     | 1.0     | 1.3     | 3.7     | 0.0     | 4.0     | 1.0     | 1.0     | 1.8     | 1.0       | 0.3       | 1.0       | 0.0     | 2.0     | 0.9  | 1.4        |            |   |  |
| Muscovite              | 0.0     | 0.3     | 0.3     | 0.5     | 1.7     | 0.0       | 0.3     | 1.0     | 0.0     | 1.0     | 1.0     | 1.0     | 2.0     | 2.4     | 0.9     | 0.3       | 1.0       | 0.0       | 1.0     | 0.5     | 0.5  | 1.0        |            |   |  |
| Biotite                | 0.0     | 0.3     | 0.0     | 0.4     | 1.3     | 0.0       | 1.0     | 0.0     | 0.0     | 0.3     | 0.0     | 0.0     | 0.0     | 0.3     | 0.3     | 1.0       | 0.1       | 0.1       | 0.0     | 0.0     | 0.0  | 0.3        | 0.2        |   |  |
| Heavy minerals         | 0.0     | 0.0     | 0.7     | 0.3     | 0.3     | 0.0       | 0.0     | 1.0     | 1.0     | 1.4     | 1.6     | 0.0     | 0.0     | 0.7     | 0.5     | 2.0       | 0.0       | 0.1       | 0.0     | 1.0     | 0.6  | 0.4        |            |   |  |
| Total                  | 53.6    | 56.6    | 57.0    | 50.1    | 41.9    | 57.8      | 56.7    | 46.0    | 53.0    | 56.4    | 48.9    | 52.9    | 46.6    | 55.8    | 52.3    | 46.1      | 50.0      | 49.7      | 49.5    | 52.6    | 49.5 | 51.8       |            |   |  |
| Q overgrowth           | 19.0    | 17.3    | 17.0    | 16.3    | 17.0    | 17.4      | 15.7    | 14.0    | 23.0    | 16.0    | 19.0    | 16.3    | 12.2    | 16.1    | 16.7    | 16.4      | 16.0      | 23.0      | 24.2    | 16.0    | 19.1 | 18.3       |            |   |  |
| Calcite                | 2.0     | 0.8     | 0.7     | 4.7     | 3.3     | 0.0       | 0.0     | 0.0     | 2.0     | 2.0     | 1.0     | 0.0     | 3.0     | 2.4     | 1.5     | 2.0       | 1.7       | 2.0       | 0.0     | 0.5     | 1.2  | 1.6        |            |   |  |
| Fe-dolomite/ankerite   | 3.0     | 1.0     | 0.0     | 0.0     | 0.0     | 0.0       | 0.7     | 0.0     | 1.0     | 0.0     | 0.0     | 2.0     | 1.0     | 4.1     | 0.8     | 5.0       | 4.0       | 1.0       | 0.0     | 1.0     | 2.2  | 2.0        |            |   |  |
| Siderite               | 2.0     | 3.0     | 1.0     | 2.7     | 3.3     | 0.0       | 3.7     | 3.9     | 1.3     | 5.0     | 2.0     | 0.0     | 2.0     | 1.7     | 2.3     | 3.0       | 1.0       | 1.0       | 1.0     | 1.0     | 1.4  | 1.9        |            |   |  |
| Kaolin                 | 2.3     | 6.7     | 1.7     | 2.3     | 6.7     | 3.0       | 5.0     | 0.0     | 1.7     | 2.7     | 4.3     | 5.7     | 8.0     | 3.4     | 3.9     | 1.5       | 3.3       | 3.3       | 1.0     | 5.0     | 2.8  | 3.0        |            |   |  |
| Pyrite                 | 0.0     | 0.0     | 0.0     | 0.3     | 1.0     | 1.0       | 0.0     | 1.3     | 0.0     | 0.3     | 0.3     | 0.0     | 3.0     | 0.0     | 0.6     | 0.0       | 0.3       | 0.1       | 0.0     | 0.2     | 0.1  | 0.2        |            |   |  |
| Chlorite               | 0.0     | 1.0     | 0.0     | 0.7     | 2.7     | 0.1       | 1.0     | 0.0     | 0.0     | 0.0     | 1.1     | 4.1     | 1.0     | 0.9     | 0.0     | 0.2       | 0.3       | 0.2       | 0.3     | 0.6     | 0.7  | 0.5        |            |   |  |
| Total cement           | 28.3    | 29.8    | 20.3    | 27.0    | 34.0    | 21.5      | 26.0    | 19.2    | 29.0    | 26.0    | 26.7    | 25.1    | 33.3    | 28.8    | 26.7    | 27.9      | 28.7      | 30.7      | 26.5    | 24.2    | 27.6 | 27.5       |            |   |  |
| Epinatatrix            | 1.7     | 1.0     | 2.0     | 3.2     | 5.7     | 1.1       | 1.3     | 0.7     | 0.0     | 1.3     | 3.1     | 4.3     | 1.6     | 0.0     | 1.9     | 3.0       | 6.3       | 0.2       | 0.3     | 3.7     | 2.7  | 2.1        |            |   |  |
| Pseudonatatrix         | 0.0     | 0.0     | 0.0     | 0.0     | 0.7     | 0.0       | 0.0     | 0.0     | 0.0     | 0.6     | 0.3     | 0.0     | 0.0     | 0.2     | 1.0     | 0.0       | 0.1       | 0.7       | 0.5     | 0.5     | 0.2  |            |            |   |  |
| Total                  | 1.7     | 1.0     | 2.0     | 3.2     | 5.7     | 1.1       | 1.3     | 0.7     | 0.0     | 1.3     | 3.1     | 4.3     | 1.6     | 0.0     | 1.9     | 3.0       | 6.3       | 0.2       | 0.3     | 3.7     | 2.7  | 2.1        |            |   |  |
| Glaucocite             | 0.0     | 0.0     | 0.7     | 0.0     | 0.7     | 0.1       | 0.3     | 16.7    | 0.0     | 0.3     | 0.7     | 0.0     | 0.0     | 3.4     | 1.8     | 7.3       | 0.0       | 12.0      | 0.3     | 3.9     | 1.9  |            |            |   |  |
| P1 porosity            | 13.7    | 10.0    | 15.7    | 14.3    | 9.7     | 16.0      | 9.0     | 12.3    | 16.7    | 11.0    | 15.0    | 16.7    | 16.9    | 9.9     | 13.3    | 11.7      | 9.0       | 12.4      | 10.0    | 15.9    | 11.8 | 12.9       |            |   |  |
| P2 porosity            | 2.7     | 2.7     | 4.3     | 5.3     | 7.3     | 3.5       | 6.7     | 5.0     | 1.3     | 4.0     | 5.0     | 0.7     | 1.7     | 2.1     | 3.8     | 3.0       | 6.0       | 6.9       | 1.0     | 2.9     | 3.5  | 3.5        |            |   |  |
| P1 + P2                | 16.4    | 12.7    | 20.0    | 19.7    | 17.0    | 19.5      | 15.7    | 17.3    | 18.0    | 15.0    | 20.0    | 17.4    | 18.6    | 12.0    | 17.1    | 14.7      | 15.0      | 19.3      | 11.0    | 18.7    | 15.7 | 16.4       |            |   |  |
| Grain size             | F1 - Fu | Fu - mu | F1 - Fu | F1 - F1 | F1 - Mu | F1 - Fu   | F1 - Fu | F1 - Mi | F1 - Mu | F1 - Fu | F1 - Crst | Fu - Crst | Fu - Crst | Fu - Mu | Fu - Mu |      |            |            |   |  |
| Sorting                | good    | good    | good    | good    | good    | good      | good    | good    | good    | good    | good    | good    | good    | good    | good    | mod.      | mod.      | mod.      | mod.    | mod.    | mod. |            |            |   |  |
| IGV                    | 36.3    | 29.0    | 36.6    | 36.7    | 36.7    | 37.5      | 31.7    | 32.0    | 35.3    | 31.7    | 39.0    | 35.3    | 35.7    | 31.0    | 34.5    | 30.3      | 31.0      | 34.6      | 36.3    | 32.1    | 32.9 | 34.5       |            |   |  |

n = number samples analyzed in the well

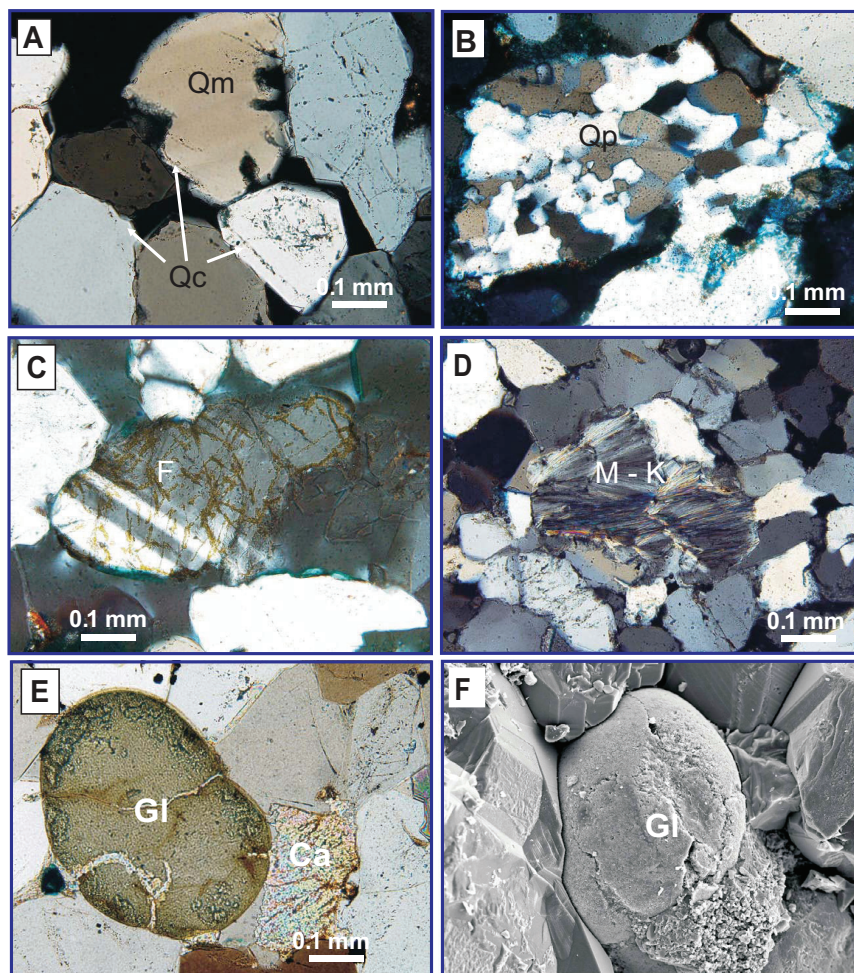


**Fig. 6.** (A) Optical photomicrographs (XPL) show quartz overgrowths (Qc) and quartz grains displaying corrosion pits. (B) Polycrystalline quartz grain. (C) Albited feldspar grain partially replaced by dolomite. (D) Kaolinitized muscovite grain in a quartzarenite. (E) Fractured glauconite grain partially replaced by calcite. (F) SEM image of glauconite grain surrounded by quartz overgrowths.

(< 2%). Minor heavy minerals such as zircon and tourmaline are present. Intrabasinal components include glauconite (Figs. 6E, F) and phosphatized micritic grains in TST and LST deposits. Glauconite occurs as scattered, commonly rounded pellets (up to 250 µm across). In thin section, these pellets may display calcite-filled cracks (Figs. 6E, F).

The composition of the T and U sandstones suggests two different source areas. Sandstones (quartz-rich and feldspar-poor) were derived from gneiss and granite-dominated stable cratonic areas and uplifted basement. Sandstones with ca. 5% lithic fragments from the LST-HST in the Napo T show evidence of provenance from recycled orogenic areas with red mudstones, sandstones and volcaniclastic rocks (Fig. 5B). Such a provenance is consistent with palaeographic reconstructions, and suggests that the Guyana Shield and the Early Triassic to Early Jurassic Santiago and Middle to Late Jurassic Chapiza Formations may constitute the main provenance for the LST and HST sandstones (Gaibor *et al.*, 2005;

Estupiñán, 2006). The Santiago Formation is composed of organic-rich shales, sandstones and limestones with a thickness varying from 1000 to 2700 m. The Santiago Formations is unconformable overlain by the continental facies of the Chapiza Formation.

#### PETROGRAPHY, GEOCHEMISTRY AND FORMATION SEQUENCE OF DIAGENETIC MINERALS

Changes occurring in marine and transitional sediments of the Napo Formation include precipitation of kaolinite as epimatrix and pore filling material, and of chlorite rims, siderite (S1) cement and pyrite. Mechanical compaction began during early diagenesis.

Kaolinite occurs as booklets and vermicular aggregates replacing feldspars as epimatrix (Tables 2, 3), and also as pore-fillings composed of thick kaolinite-dickite crystals corroding quartz overgrowths (Figs. 7A, C, and D).

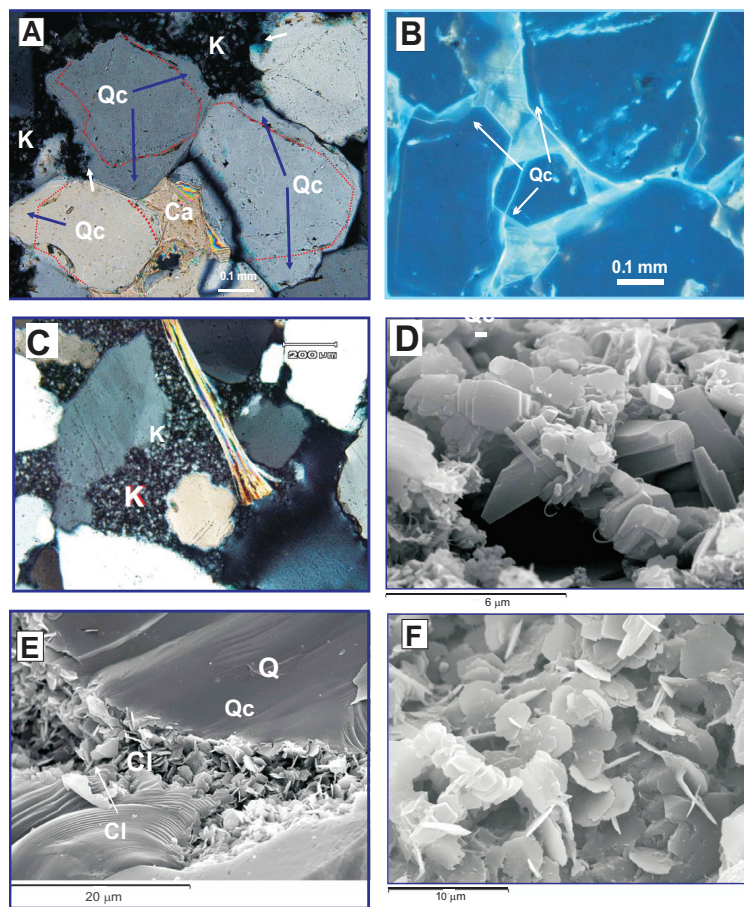


**Fig. 7.** (A) Optical photomicrograph (XPL) showing broad rims of quartz overgrowths (Qc) partially corroded by kaolinite pore-filling and by calcite cement (Ca). (B) Fluorescence microscopy image showing quartz overgrowths and some fractures filled with bitumen which cut detrital grains. (C) Optical photomicrograph (crossed nicols) of pervasive kaolinite (K) filling pore between corroded quartz overgrowths and muscovite. (D) SEM image of blocky kaolinite transformed to fibrous illite. (E) and (F) SEM images of chlorite clay rim pre-dating quartz overgrowth.

Dickite was distinguished from kaolinite by SEM and XRD analyses. Dickite shows two strong reflections (2.50 and 2.32 Å), and under SEM occurs as blocky crystals that are much thicker (5–10 µm) than kaolinite with a vermicular stacking pattern containing etched kaolinite remnants.

Authigenic illite is rare and occurs as replacement after kaolinite and as fibrous to lamellar crystals (Fig. 7D). Muscovite is commonly replaced by kaolinite (Figs. 6D and 7C). The dissolution of framework grains and the formation of kaolinite in both sandstones occur in fluvial and shallow-marine LST deposits.

Chlorite is a minor constituent in the sandstones (Tables 2, 3). It occurs as a grain coating and is composed of pseudo-hexagonal platelets that are arranged perpendicular to grain surfaces (Figs. 7E, F). Chlorite cement may have formed through diagenetic transformation of precursor clays (Morad *et al.*, 2000) e.g. berthierine, which was precipitated in mixed marine-meteoric waters in tidal channel and estuarine settings. Chlorite is engulfed by quartz overgrowths, followed by dolomite, calcite and

siderite (S2) cements. Chlorite is more abundant in the LST-HST deposits within wave and tidal influenced sandstones than in fluvial-incised valley deposits (LST), and is not present in transgressive (TST) sandstones.

Two generations of siderite cement were recognised: S1 and S2. *Siderite S1* occurs as small lenticular crystals (10–50 µm) and as euhedral rhombs filling intergranular pores. In some cases, it replaces feldspars and mud intraclasts (Figs. 8A, B). Under CL, both siderites are non-luminescent owing to Fe-quenching. Siderite S1 is partially replaced by Fe-dolomite (Fig. 8B), calcite or ankerite. Siderite S1 predates quartz cement (Fig. 8A). However, the quartz cement shows “embayment” of the later siderite, S2. The average chemical composition of siderite S1 is  $(\text{Fe}_{81.8}\text{Mg}_{10.2}\text{Mn}_{0.9}\text{Ca}_{7.1})\text{CO}_3$  (Table 4). Some siderites have values of up to 99%  $\text{FeCO}_3$ , and relatively high Mn contents (>3.9 mol) (Fig. 9). Siderite S1 has the highest Mn content in LST and TST deposits (Table 4).  $\delta^{13}\text{C} \text{‰ PDB}$  values of siderite S1 vary between -3.6 and -2.6‰, and  $\delta^{18}\text{O}$  between -6.3 and -3.2‰ in

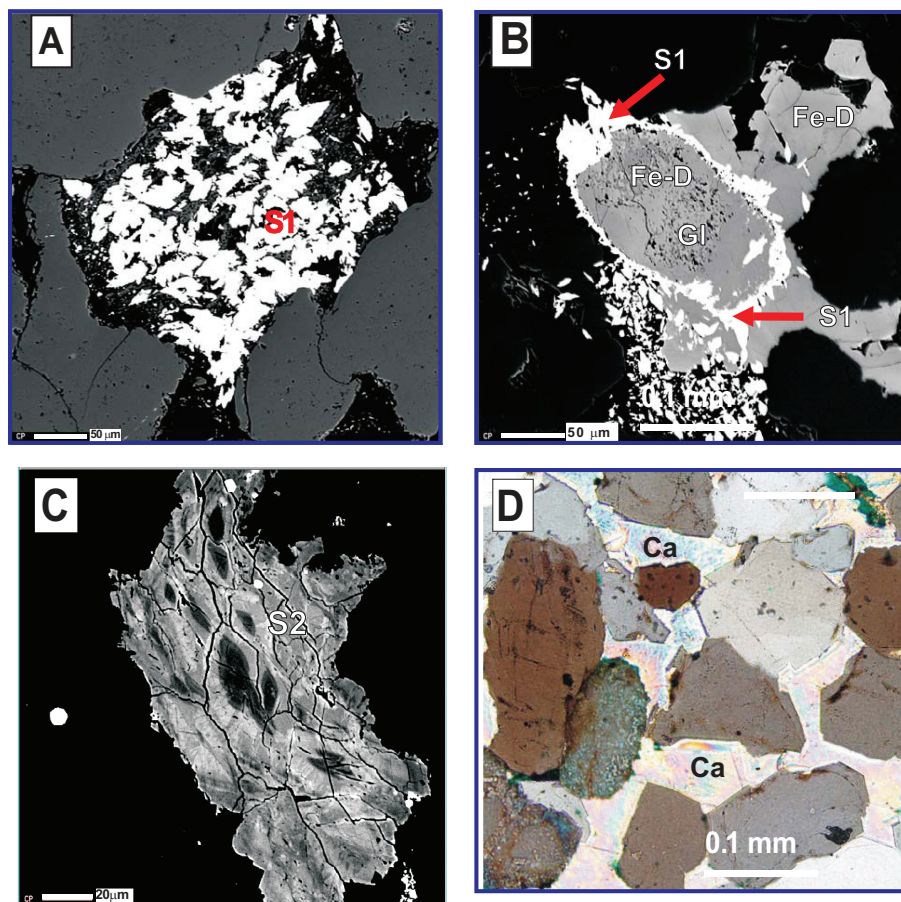


**Fig. 8. (A, B and C) BSE images. (A) K-feldspar replaced by thin lens of siderite S1. (B) Fe-dolomite engulfing siderite lens and small rhombs of siderite S1. (C) Detail of siderite S2 replacing S1 and showing complex zonation. (D) Optical photomicrograph (crossed nicols) of poikilotopic calcite cements post-dating quartz overgrowths.**

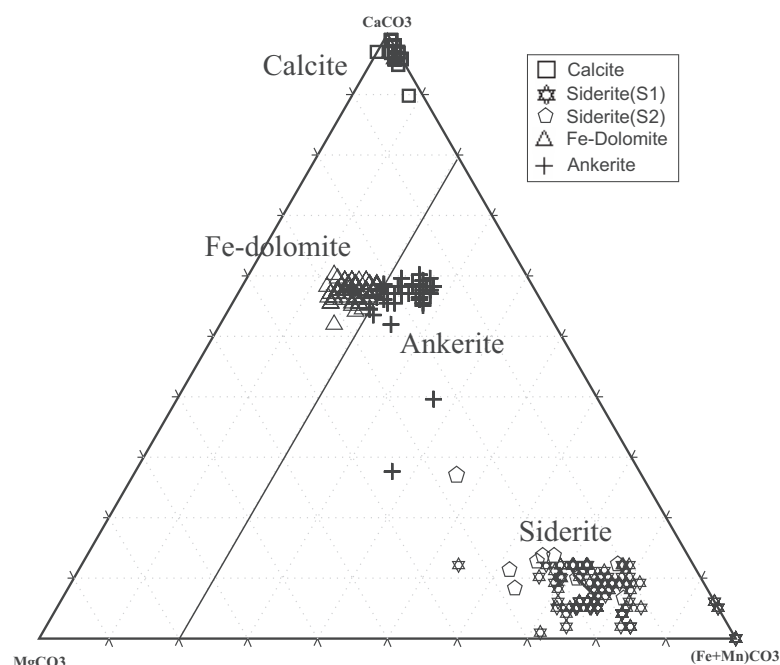


**Fig. 9. Ternary diagram showing the chemical composition of representative carbonate cements (Ca, Fe+Mn, Mg)CO<sub>3</sub>, from the Napo Formation. Note that S1 and S2 siderites are characterized by a relatively similar composition due to the complexity of analyzing the small S1 crystals.**

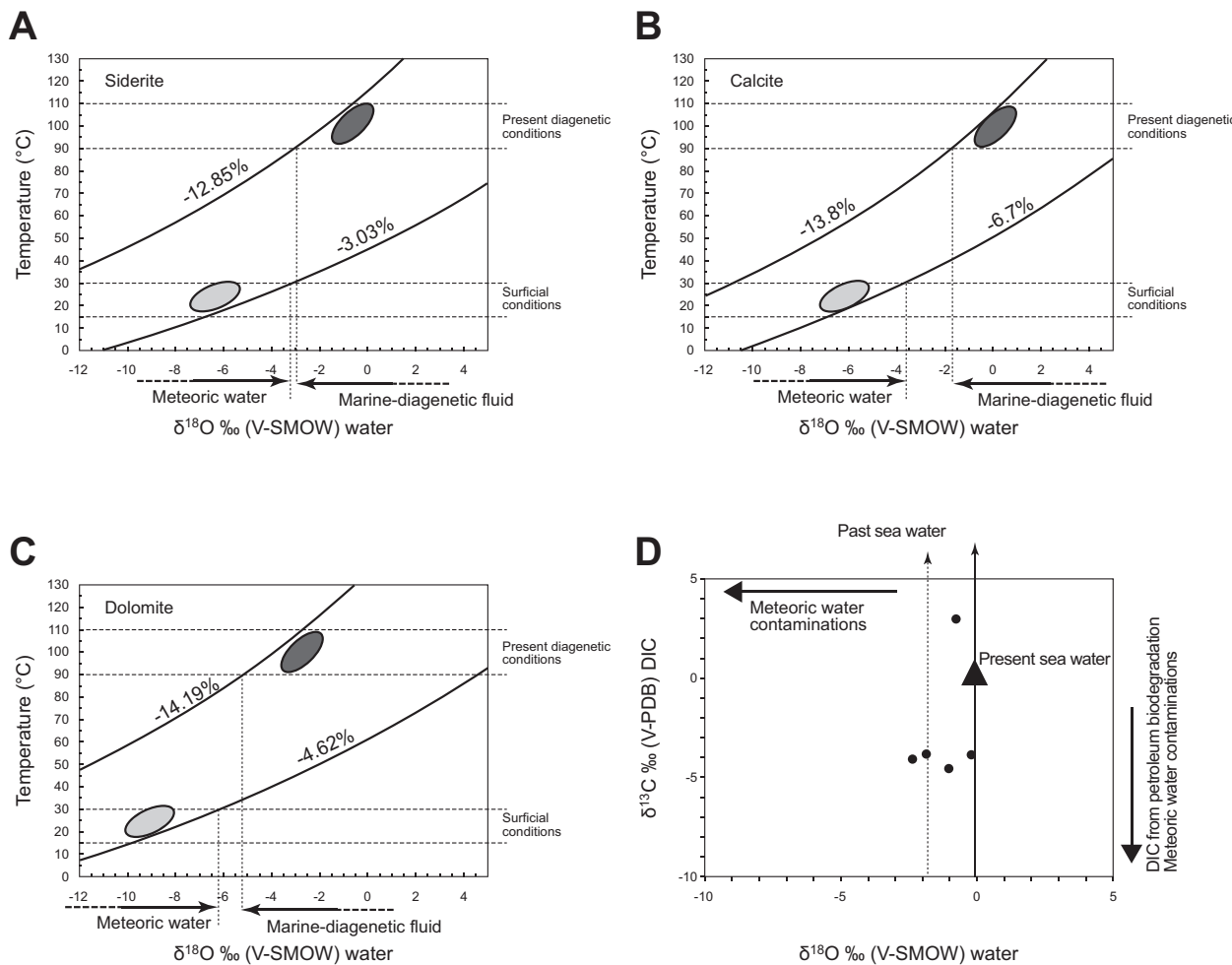


**Fig. 10. (A-C).** Diagrams showing the range of temperature and isotopic values of the pore fluids that limit the precipitation of the analyzed siderites, calcite and dolomite. The curves represent the theoretical temperature of carbonates in equilibrium with different waters. Maximum and minimum  $\delta^{18}\text{O}$  values of siderite are plotted. Equations from Carothers *et al.* (1988) for calcite and O'Neil *et al.* (1969) and Irwin and Coleman (1977) for dolomite were used to calculate the isotopic fractionation in the siderite-water systems. (D). Diagram showing the isotopic analyses from formation water obtained from the wells studied (modified from Estupiñan *et al.*, 2007).

the T and U sandstones (Fig. 10A; Table 4). Average stable isotope values are quite similar in the U and T sandstones.

*Pyrite* is a minor constituent in all the studied sandstones (Tables 2, 3).

*Quartz* cement occurs as overgrowths in all the Napo Formation samples analysed (avg. 16% in the U and 12% in the T sandstones). The irregular forms of the quartz overgrowth may be related to the incorporation of kaolinite pore-fill (Fig. 7A). Some overgrowths have concave-convex contacts, probably the result of mild pressure solution. This may also be due to intergrowth of quartz cement crystals. Under fluorescent microscopy, the boundaries between quartz grains and overgrowths may show traces of oil. Oil traces were also observed in healed fractures (Fig. 7B). Quartz cement was formed after siderite S1 and chlorite rim cement (Figs. 7E, F and 8A).

Quartz cement in turn predates calcite, dolomite, siderite S2 and dickite cements.

Irregularly shaped *fluid inclusions* (FI) occur in the quartz cement and are up to 20  $\mu\text{m}$  in diameter. They are located within quartz overgrowths or in boundary zones with detrital quartz grains. Aqueous inclusions have salinities of 20.5 - 23.17 eq. NaCl and Th values ranging from 80-190°C with a mode at around 130°C (Fig. 11). Bottom-hole temperatures and the modelled burial and thermal history of the basin (Fig. 3) suggest that the quartz cement began to precipitate at around 80°C, reaching a maximum between 120 and 140°C. The high Th values (140-190°C) do not fit into this temperature pattern, and may possibly have been measured accidentally on transported quartz grains from Lower Cretaceous and Jurassic sandstones from the source areas (Hollín, Chapiza and Santiago Formations).

**Table 4. Chemical composition based on microprobe analyses and isotopic ratios of representative carbonate cements of the T and U reservoir sandstones of the Napo Formation.**

| Sandstone<br>Samples | LST  |      |               |      | LST-HST |      |               |     | TST  |      |      |      | $d^{13}\text{C}$<br>(‰ V-PDB) |       |       |       | $d^{18}\text{O}$<br>(‰ V-PDB) |   | Remarks |                  |
|----------------------|------|------|---------------|------|---------|------|---------------|-----|------|------|------|------|-------------------------------|-------|-------|-------|-------------------------------|---|---------|------------------|
|                      | Mg   | Ca   | $\text{CO}_3$ | Mn   | Mg      | Ca   | $\text{CO}_3$ | Mn  | Fe   | Sr   | Mg   | Ca   | $\text{CO}_3$                 | Mn    | Fe    | Sr    |                               |   |         |                  |
| <b>U Sandstone</b>   |      |      |               |      |         |      |               |     |      |      |      |      |                               |       |       |       |                               |   |         |                  |
| <b>SIDERITE S1</b>   | 18.6 | 11.6 | 0.9           | 69.1 | 0.0     |      |               |     | 12.4 | 9.2  | 0.9  | 77.5 | 0.0                           | -3.4  | -3.7  |       |                               |   |         |                  |
| average              | 19.3 | 12.2 | 0.7           | 70.5 | 0.0     |      |               |     | 13.9 | 10.9 | 1.0  | 80.0 | 0.0                           | -3.6  | -4.3  |       |                               |   |         |                  |
| maximum              | 17.8 | 11.0 | 0.6           | 67.8 | 0.0     |      |               |     | 11.2 | 7.0  | 0.7  | 75.4 | 0.0                           | -3.2  | -3.2  |       |                               |   |         |                  |
| <b>SIDERITE S2</b>   | 23.8 | 13.9 | 0.4           | 61.8 | 0.0     |      |               |     |      |      |      |      |                               | -8.5  | -10.8 |       |                               |   |         | Rhombic siderite |
| average              | 27.6 | 27.0 | 0.8           | 66.5 | 0.0     |      |               |     |      |      |      |      |                               | -10.0 | -11.4 |       |                               |   |         |                  |
| maximum              | 20.7 | 8.0  | 0.2           | 45.8 | 0.0     |      |               |     |      |      |      |      |                               | -7.1  | -10.3 |       |                               |   |         |                  |
| <b>CALCITE</b>       | 3.8  | 96.5 | 0.1           | 0.5  | 0.1     |      |               |     | 1.3  | 95.4 | 1.0  | 2.3  | 0.0                           | -3.5  | -11.4 |       |                               |   |         |                  |
| average              | 4.0  | 97.0 | 1.3           | 0.9  | 0.1     |      |               |     | 1.9  | 97.6 | 1.3  | 3.1  | 0.0                           | -3.5  | -10.5 |       |                               |   |         |                  |
| maximum              | 3.7  | 96.0 | 0.1           | 0.2  | 0.1     |      |               |     | 0.3  | 94.2 | 0.3  | 1.4  | 0.0                           | -9.3  | -13.8 |       |                               |   |         |                  |
| <b>Fe-DOLOMITE</b>   | 26.6 | 57.3 | 0.4           | 15.6 | 0.0     | 26.6 | 56.6          | 0.6 | 16.1 | 0.0  |      |      |                               | -4.0  | -9.2  |       |                               |   |         |                  |
| average              | 31.6 | 59.7 | 0.9           | 18.8 | 0.1     | 30.3 | 59.2          | 1.4 | 19.0 | 0.1  |      |      |                               | -3.3  | -4.6  |       |                               |   |         |                  |
| maximum              | 23.1 | 51.8 | 0.2           | 12.7 | 0.0     | 22.9 | 54.2          | 0.3 | 12.4 | 0.0  |      |      |                               | -6.2  | -14.2 |       |                               |   |         |                  |
| <b>ANKERITE</b>      | 23.2 | 52.7 | 0.8           | 23.2 | 0.0     | 22.9 | 52.1          | 0.9 | 21.1 | 0.0  |      |      |                               | -     | -     |       |                               |   |         |                  |
| average              | 27.5 | 57.2 | 1.4           | 48.7 | 0.1     | 25.9 | 57.1          | 1.0 | 23.3 | 0.0  |      |      |                               | -     | -     |       |                               |   |         |                  |
| maximum              | 20.0 | 21.9 | 0.2           | 19.3 | 0.0     | 20.0 | 51.9          | 0.7 | 19.3 | 0.0  |      |      |                               | -     | -     |       |                               |   |         |                  |
| <b>T Sandstone</b>   |      |      |               |      |         |      |               |     |      |      |      |      |                               |       |       |       |                               |   |         |                  |
| <b>SIDERITE S1</b>   | 0.1  | 2.7  | 0.1           | 97.2 | 0.0     | 9.5  | 5.0           | 1.0 | 83.4 | 0.0  |      |      |                               | -2.7  | -4.7  |       |                               |   |         |                  |
| average              | 0.1  | 5.2  | 0.1           | 99.8 | 0.0     | 16.4 | 8.6           | 3.9 | 99.9 | 0.2  |      |      |                               | -2.8  | -6.3  |       |                               |   |         |                  |
| maximum              | 0.0  | 0.1  | 0.1           | 94.5 | 0.0     | 0.0  | 0.0           | 0.0 | 71.5 | 0.0  |      |      |                               | -2.6  | -3.0  |       |                               |   |         |                  |
| <b>SIDERITE S2</b>   | 17.2 | 7.2  | 0.4           | 73.7 | 0.0     |      |               |     |      |      |      |      |                               | -6.5  | -12.4 |       |                               |   |         |                  |
| average              | 33.7 | 13.0 | 2.0           | 94.5 | 0.1     |      |               |     |      |      |      |      |                               | -9.6  | -13.1 |       |                               |   |         |                  |
| maximum              | 0.1  | 1.2  | 0.0           | 52.5 | 0.0     |      |               |     |      |      |      |      |                               | -3.4  | -11.6 |       |                               |   |         |                  |
| <b>CALCITE</b>       | 0.6  | 97.2 | 0.3           | 1.9  | 0.0     | 0.7  | 96.5          | 0.6 | 2.2  | 0.0  | 0.8  | 96.2 | 0.6                           | 2.4   | 0.0   | -7.7  | -10.5                         |   |         |                  |
| average              | 0.7  | 97.5 | 0.3           | 2.0  | 0.1     | 2.5  | 98.5          | 1.6 | 7.9  | 0.1  | 2.5  | 98.5 | 1.6                           | 7.9   | 0.1   | -1.3  | -6.7                          |   |         |                  |
| maximum              | 0.5  | 97.0 | 0.3           | 1.7  | 0.0     | 0.2  | 89.0          | 0.1 | 1.0  | 0.0  | 0.2  | 89.0 | 0.4                           | 1.0   | 0.0   | -12.7 | -11.6                         |   |         |                  |
| <b>Fe-DOLOMITE</b>   | 26.7 | 56.0 | 0.3           | 17.0 | 0.0     | 24.9 | 57.6          | 0.4 | 17.2 | 0.0  |      |      |                               | -4.7  | -9.4  |       |                               |   |         |                  |
| average              | 27.7 | 57.4 | 0.4           | 19.0 | 0.1     | 27.3 | 59.0          | 0.5 | 19.4 | 0.0  |      |      |                               | -3.4  | -4.8  |       |                               |   |         |                  |
| maximum              | 25.4 | 54.8 | 0.2           | 16.0 | 0.0     | 22.5 | 53.9          | 0.2 | 15.5 | 0.0  |      |      |                               | -7.1  | -13.7 |       |                               |   |         |                  |
| <b>ANKERITE</b>      | 19.6 | 56.9 | 0.7           | 22.8 | 0.0     | 18.4 | 57.6          | 0.8 | 23.2 | 0.0  | 16.1 | 57.3 | 2.1                           | 24.6  | 0.0   | -     | -                             | - | -       |                  |
| average              | 25.5 | 59.7 | 1.0           | 26.9 | 0.0     | 21.2 | 59.6          | 1.9 | 25.8 | 0.0  | 17.6 | 59.2 | 3.2                           | 25.5  | 0.0   | -     | -                             | - | -       |                  |
| maximum              | 16.7 | 54.3 | 0.5           | 19.7 | 0.0     | 15.5 | 56.2          | 0.5 | 19.7 | 0.0  | 14.7 | 55.0 | 1.3                           | 22.3  | 0.0   | -     | -                             | - | -       |                  |

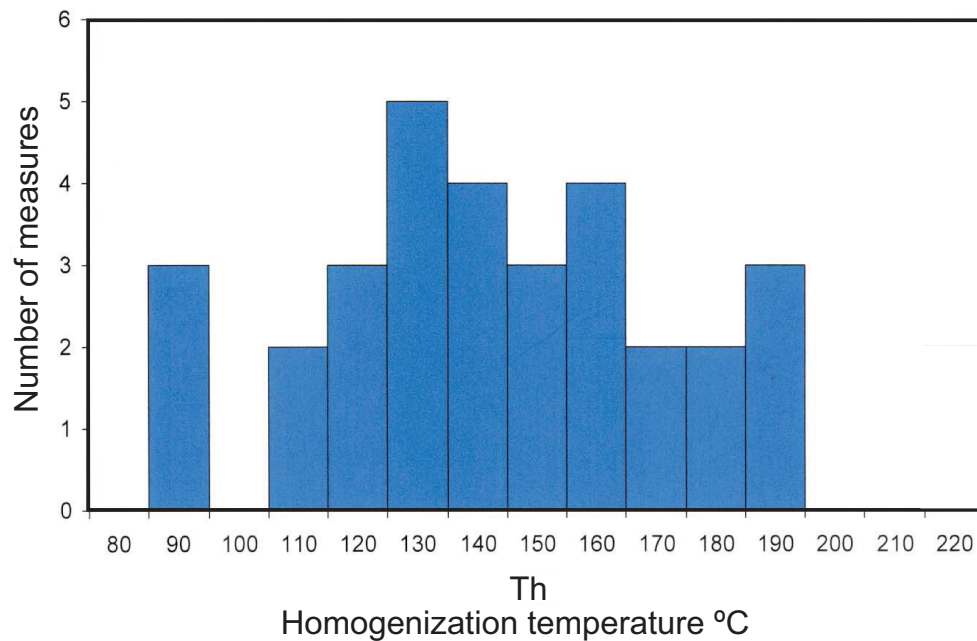


**Fig. 11. Homogenization temperature measurements on fluid inclusions occurring along boundaries between quartz grains and overgrowths in selected quartzarenite samples from the Napo Formation U and T member sandstones.**

Siderite S2 occurs as large rhombic crystals varying from 20 to 100 µm. The average composition of siderite S2 is  $(\text{Fe}_{67.8}\text{Mg}_{20.5}\text{Mn}_{0.8}\text{Ca}_{11.1})\text{CO}_3$  (Table 4; Fig. 9). Siderite S2 has a higher content of Mg and lower content of Fe and Mn (< 1%) than eodiagenetic siderite S1, and its chemical composition suggests sideroplesite (5-30 mole%  $\text{MgCO}_3$ ) (Table 4). Siderite S2 shows Mg zoning (Fig. 8C). Mg is higher in inner zones than in outer zones (22 mol % and 10 mol %, respectively).

The  $\delta^{13}\text{C}$  PDB for siderite S2 varies from -10.0 to -3.4‰, and  $\delta^{18}\text{O}$  PDB from -13.1 to -10.3‰ PDB. The siderite (S1+S2)  $\delta^{18}\text{O}$  V-SMOW values vary between -12.85 and -3.03‰ (Fig. 10A; Table 4). Fig. 10A shows that the temperatures of the two siderite phases are in equilibrium with water of different isotopic compositions. Nevertheless, the two siderite generations plot close to each other on a compositional ternary diagram (Fig. 9).

Calcite cement occurs as scattered patches (up to 100 µm) in the LST and TST sandstones. It forms poikilotopic crystals (50-100 µm) in LST deposits (Fig. 8D) with an average content of 5% of the bulk sample (Tables 2, 3). This type of calcite is non-luminescent probably because of Fe-quenching. Calcite replaces feldspars and post-dates quartz overgrowth development and chemical compaction. Detrital quartz and its overgrowths are clearly corroded by this phase of calcite generation (Fig. 8D). Glauconite is partially or totally replaced by calcite (Fig. 6E) and pyrite is included in this calcite cement.

The average composition of calcite cement in the LST sandstones is  $(\text{Ca}_{95.8}\text{Fe}_{2.4}\text{Mg}_{1.1}\text{Mn}_{0.8})\text{CO}_3$  (Table

4). The intergranular volume (IGV) in these sandstones is over 30% (Tables 2, 3). The Mg content is 3.8 mol% avg. in the U sandstones and 0.6 mol% avg. in the T sandstones (Table 4). The Sr content varies from below the detection limit to 0.2 mol‰ (Table 4).

$\delta^{13}\text{C}$  values of calcite cement vary between -9.3 and -3.5‰ and, and  $\delta^{18}\text{O}$  between -13.8 and -10.5‰ PDB.  $\delta^{13}\text{C}$  values in the T sandstones vary between -12.7 and -1.3 ‰, and  $\delta^{18}\text{O}$  between -11.6 and -6.7‰ PDB. The calcite  $\delta^{18}\text{O}$  V-SMOW shows values varying from -13.8 to -6.7‰ (Fig. 10B; Table 4).

*Ferroan dolomite/ankerite*, which fills intergranular pores and replace the framework grains and quartz overgrowths, occur in numerous patches (Figs. 12B, C). The abundance of this mineral phase ranges from zero to 2.3%. Fe-dolomite and ankerite replace siderite S1 and enclose siderite S2 (Fig. 12C), forming intergranular mosaics of subehedral, non-luminescent crystals, up to 100 µm in size. The sweeping extinction and the irregularly curved crystal boundaries provide evidence of void-filling, coarse crystalline saddle dolomite post-dating quartz overgrowths (Fig. 12A). In some cases, this cement is mixed with calcite and siderite S2, and diagenetic sequences are difficult to distinguish (Fig. 12C).

The chemical composition of Fe-dolomite in HST tidal bar sandstones is  $(\text{Mg}_{26.2}\text{Fe}_{16.5}\text{Mn}_{0.4}\text{Ca}_{56.9})\text{CO}_3$ , and ankerite  $(\text{Mg}_{21}\text{Fe}_{22.6}\text{Mn}_{0.8}\text{Ca}_{54.8})\text{CO}_3$  (Table 4). The Fe-dolomite/ankerite displays patchy zonation in BSE images, with variations in the  $\text{FeCO}_3$  content ranging from 12-28 mol% (Fig. 12D). The  $\delta^{13}\text{C}$  values in the

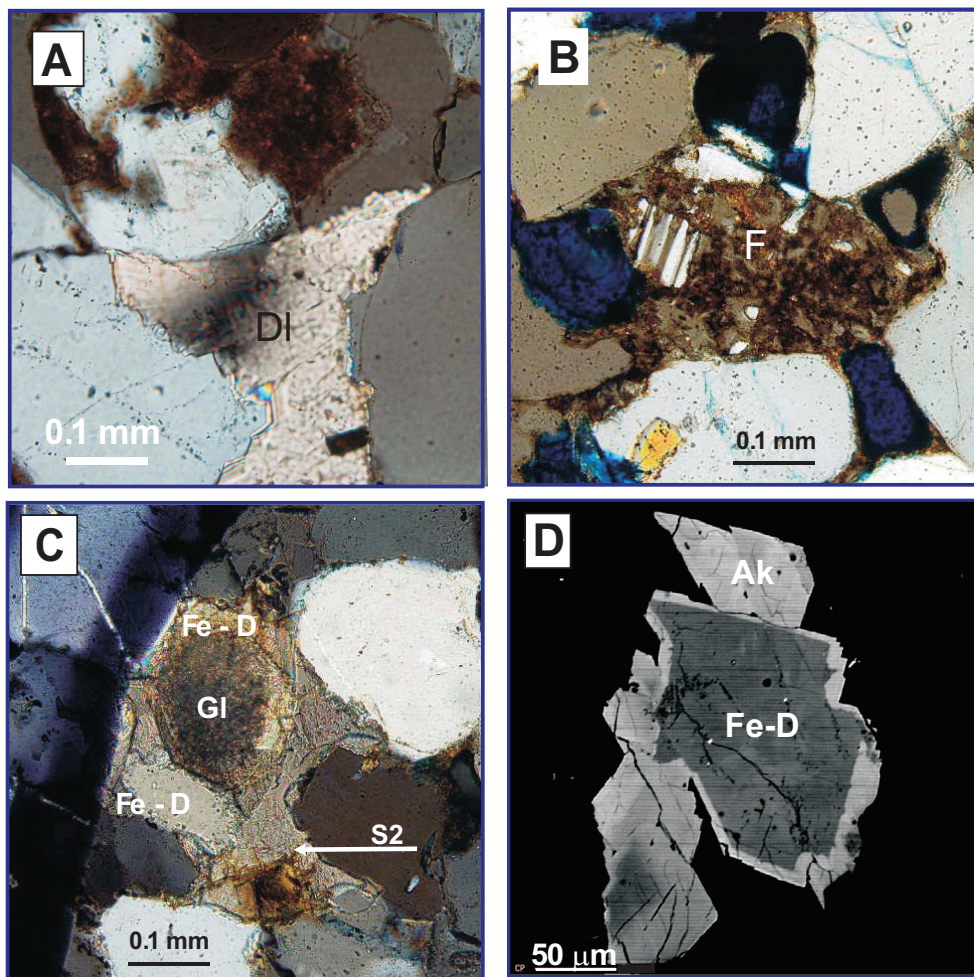


**Fig. 12.** Optical photomicrographs (XPL): (A) Ferroan saddle Fe-dolomite replacing quartz overgrowth. Individual dolomite crystal outlines are poorly developed but sweeping extinction is widespread. (B) Patches of Fe-dolomite partially replacing K-feldspar. (C) Fe-dolomite post-dates quartz overgrowth replacing a glauconite grain. (D) SEM image. Patches of Fe-dolomite post-date quartz overgrowth. Ak: ankerite.

Napo U sandstones range from -6.2 to -3.3‰, and  $\delta^{18}\text{O}$  from -14.2 to -4.6‰ PDB. The  $\delta^{13}\text{C}$  values in the Napo T sandstones vary between -7.1 and -3.4‰, and  $\delta^{18}\text{O}$  between -13.7 and -4.8‰ PDB. Dolomite  $\delta^{18}\text{O}$  V-SMOW values vary from -14.19 to -4.62‰ (Fig. 10C). These carbonate cements are more abundant in TST deposits in both U and T sandstones than in other intervals (Table 5).

#### POROSITY EVOLUTION

Porosity in the sandstones includes both primary (intergranular) (Figs 13A, B) and secondary (mouldic, intergranular and oversized) types, indicating dissolution of whole grains and grain-replacing cements (Figs 13C, D).

Mouldic porosity is caused by partial or complete dissolution of feldspars, particularly plagioclase. The other types of secondary porosity are related to the dissolution of carbonate cements and replacements. The average original porosity of the T and U

sandstones is ca. 40%, estimated from a Trask sorting coefficient of 1.5 (moderately to well-sorted sandstones) and the detrital quartz content (after Scherer, 1987).

Primary plus secondary porosity are fairly similar in all the systems tract deposits (average primary porosity 11% and secondary 5%). Secondary pores have good connectivity with depositional intergranular pores (Fig. 13C). The intergranular porosity (P1) can be used to calculate the intergranular volume (IGV= total cement + intergranular porosity). These values are integrated to predict the results of combined porosity loss due to compaction and cementation. These parameters indicate that the loss of porosity related to depositional facies was intense because of cementation rather than compaction (Fig. 14, from Houseknecht, 1988, modified by Ehrenberg, 1989; Tables 2 and 3). In LST-HST and LST sandstone from the T interval, the porosity loss was more severe owing to meteoric water percolation (Ketzer *et al.*, 2003a) than in TST transgressive systems tract deposits.

## U Sandstone

|             | TST                 | LST-HST            | LST            |
|-------------|---------------------|--------------------|----------------|
| EOGENETIC   | -----               | chlorite ▲▲▲       | chlorite ▲▲    |
|             | kaolinite ▲▲        | kaolinite ▲▲▲      | -----          |
|             | S1 siderite ▲▲▲     | -----              | siderite ▲▲    |
| MESOGENETIC | S2 siderite ▲▲      | -----              | S2 siderite ▲▲ |
|             | calcite ▲▲          | -----              | calcite ▲▲▲    |
|             | fe-dol/ankerite ▲▲▲ | fe-dol/ankerite ▲▲ | -----          |
|             | quartz ▲▲▲          | quartz ▲▲▲         | quartz ▲▲▲     |
|             | dickite ▲▲          | dickite ▲▲         | dickite ▲▲     |

## T Sandstone

|             | TST                 | LST-HST            | LST               |
|-------------|---------------------|--------------------|-------------------|
| EOGENETIC   | -----               | chlorite ▲▲▲       | chlorite ▲▲       |
|             | kaolinite ▲▲        | kaolinite ▲▲▲      | -----             |
|             | S1 siderite ▲▲      | S1 siderite ▲▲▲    | S1 siderite ▲▲    |
| MESOGENETIC | S2 siderite ▲▲      | -----              | S2 siderite ▲▲    |
|             | calcite ▲▲          | calcite ▲▲         | calcite ▲         |
|             | fe-dol/ankerite ▲▲▲ | fe-dol/ankerite ▲▲ | fe-dol/ankerite ▲ |
|             | quartz ▲▲▲          | quartz ▲▲▲         | quartz ▲▲▲        |
|             | dickite ▲▲          | dickite ▲▲         | dickite ▲▲        |

Key: abundant ▲▲▲ frequent ▲▲ rare ▲

**Table 5. Semi-quantitative distribution of main diagenetic products in the U and T sandstones within a sequence stratigraphic context. S1 and S2 siderite was quantified from thin section analyses (not point-counting) in plain light and by microprobe analysis. The distributions of kaolinite and dickite were determined in a similar fashion.**

Secondary intergranular, intragranular and mouldic pores due to partial and total dissolution of feldspar grains and carbonate cement were enhanced by up to ca. 6% in total porosity in the U interval and ca. 3% in the T interval, consistent with the fact that the T sandstones were more deeply buried than the U sandstones (Fig. 4).

## DISCUSSION

### Diagenetic alterations associated with sequence stratigraphy

Diagenetic cement sequences can provide valuable information about the geochemical evolution of pore waters, although there are difficulties due to the presence of multiple cement generations and subsequent dissolution (Morad, 1998).

In this study, the abundance of three eogenetic minerals appears to be related to sequence stratigraphy (Table 5):

Chlorite in both the U and T sandstones is absent in TST deposits, abundant in LST-HST deposits and frequent in LST deposits.

Kaolinite occurs frequently in TST deposits and is abundant in LST-HST but is not present in LST deposits.

By contrast, S1 siderite occurs in variable amounts in the different system tracts in the U and T sandstones. In the U sandstones, S1 is abundant in TST deposits, absent in LST-HST deposits and frequent in LST deposits. In the T sandstones, S1 is frequent in TST deposits, abundant in LST-HST, and frequent in LST deposits.

Siderite S1 has values of up to 99% FeCO<sub>3</sub> and also high values of Mn (3.9 %) in the wave-tidal (LST-HST) T sandstones (Table 4), suggesting that the siderite cement precipitated from reducing meteoric fluids, possibly near the water-sediment interface or in the phreatic zone (Mozley, 1989; Morad, 1998; Morad *et al.*, 2000). These authors reported that siderite with more than 90% FeCO<sub>3</sub> and more than 2.0% MnCO<sub>3</sub> indicates eogenetic processes in lowstand deposits. However, it was observed that S2 siderite and Fe-dolomite/ankerite have replaced S1 siderite in places. This means that the original amount of siderite S1 may have been higher, and its relationship

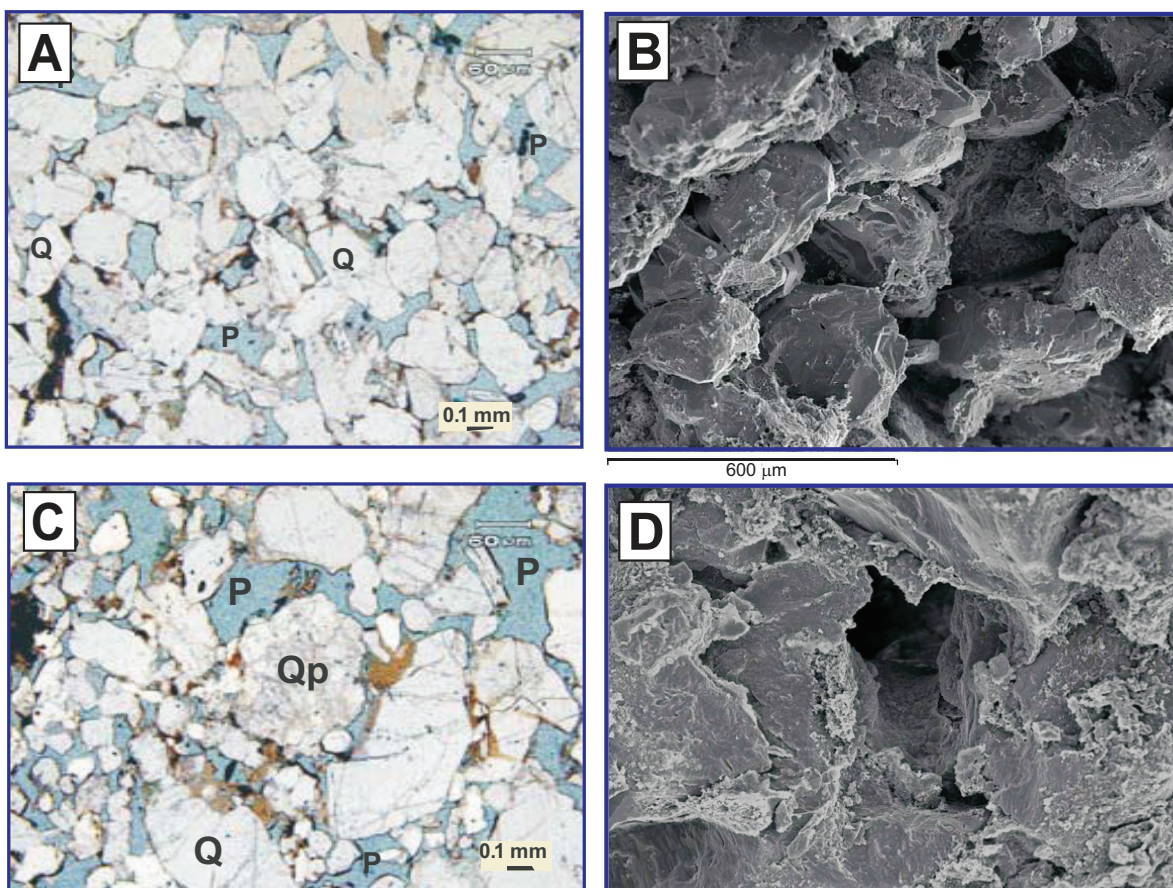


**Fig. 13. (A and B)** Optical photomicrograph (PPL) and SEM image, respectively, showing intergranular primary porosity. **(C and D)** Secondary porosity (intragranular and oversized pores coated by bitumen) related to partially dissolved feldspar and carbonate cement-replacements.

to the sequence strigraphic framework may have been different.

A similar problem applies to kaolinite which occurs as booklets and vermicular aggregates replacing feldspar grains and as kaolinite/dickite pore-fillings. Later kaolinite has replaced at least some of the early kaolinite. Only chlorite seems to have a good relationship with systems tracts without later partial replacement by other mesogenetic minerals.

Mesogenetic alterations are somewhat different in the T and U sandstones (Table, 5; Figs, 15 and 16). In the T sandstones, only Fe-dolomite/ankerite is abundant in TST deposits, while calcite, quartz and mesogenetic kaolinite/dickite occur in similar quantities in all systems tracts. In the U sandstones, calcite occurs frequently only in LST deposits but is absent in LST-HST. Fe-dolomite is common in TST deposits, comparable to the T unit. Quartz and dickite are equally distributed in all system tracts (quartz precipitation at  $>70^{\circ}\text{C}$ , after Morad *et al.*, 2000). S2 siderite is present in TST and LST deposits but is absent in LST-HST in both U sandstones and T sandstones.

Mesogenetic minerals such as S2 siderite, calcite and Fe-dolomite show negative oxygen isotope ratios from -11 to -9‰, suggesting meteoric mixing and

higher temperatures due to deep burial.

El-Ghali *et al.* (2008) found a fairly systematic link of mesogenetic alterations including quartz overgrowths and illite to LST sandstones. This could not be recognised in this study. However, the Fe-dolomite seemed to have been preferentially formed in TST deposits in both the U and T sandstones.

Mg-siderite (S2) is the last carbonate phase. The higher content of Mg in siderite S2 may be related to the maturity of certain types of algal organic matter in the interbedded source rocks (Desborough, 1978). The incorporation of Mg into the siderite network occurs at higher temperatures (Mozley and Burn, 1993; Smith and Ehrenberg, 1989).

#### Porosity evolution in the U and T Sandstones

Major porosity-reducing processes in the Napo Formation sandstones are cementation by quartz overgrowths, carbonates and various kaolinite/dickite phases, mechanical compaction, and to a lesser degree, chemical compaction (pressure solution) expressed as occasional concave/convex grain contacts. There is no clear evidence that chlorite coating of grains has retarded pressure solution.

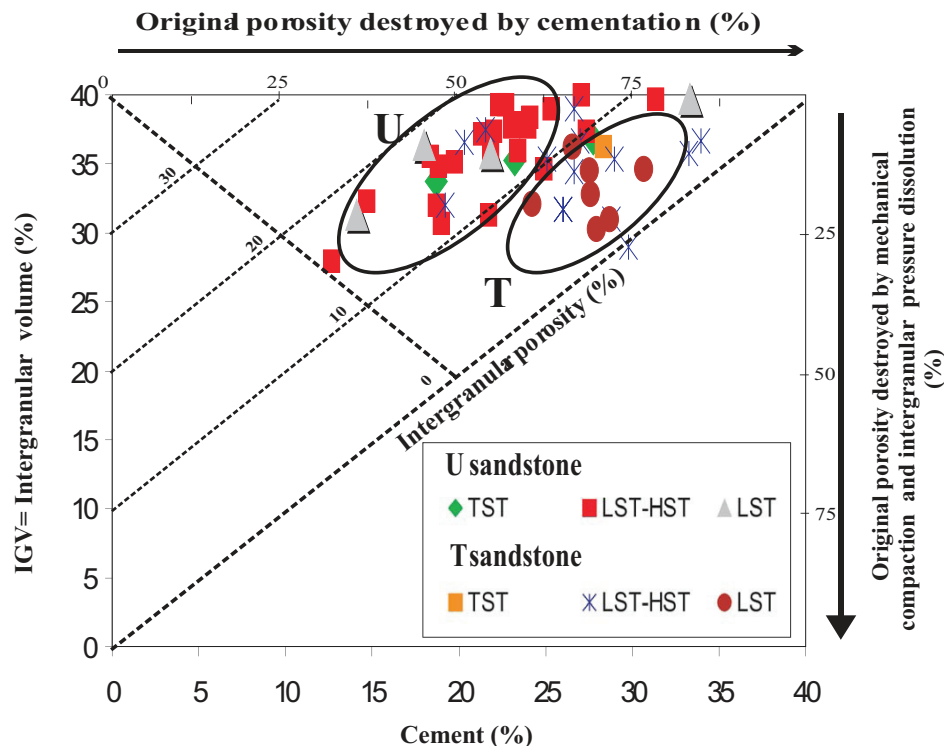


**Fig. 14.** Plot of intergranular volume (IGV) versus volume of cement (Houseknecht, 1987; modified by Ehrenberg, 1989) of 52 sandstone samples from the Cretaceous Napo Formation U and T members. Cementation was more important than compaction in destroying primary porosity in the fluvial and marine sandstones. Porosity loss was more severe in LST sandstones from the U member and LST-HST sandstones from the T member than in TST deposits (see text for details).

Instead, chlorite is commonly engulfed in quartz cement. Since little silica is provided from pressure solution, it was probably derived from interbedded shales (e.g. Galloway, 1984; Byorlykke, 1999).

Porosity in both sandstone units consists of remaining primary porosity (P1) and secondary porosity (P2) due to leaching of cement and chemically unstable grains such as feldspars. Both primary and secondary porosity are similar in all systems tract deposits. However, the average P1 porosity is approx. 10% in the U sandstones and 13% in the T sandstones; while the average secondary porosity is 6% in the U sandstones and only 3.5% in the T sandstones. Total porosity is approx. 16% in both units. The difference in primary and secondary porosity is statistically significant. Secondary porosity can mostly be linked to the remaining amounts of feldspar (U sandstones: 2.8%; T sandstones: 4.6%: Tables 2, 3). There was therefore more leaching of feldspars in the U sandstones than in the T sandstones, independent of system tracts.

Secondary porosity due to leaching occurred during late stage diagenesis. Thermal degradation of carboxylic acids produced CO<sub>2</sub> and methane, lowered pH levels and induced cement dissolution, which may account for this leaching process (c.f. Schmidt and McDonald, 1979; Surdam *et al.*, 1984; Wilkinson and Haszeldine, 1996). This dissolution phase may have

coincided with hydrocarbon expulsion and migration in the Oriente Basin in Miocene times (ca. 8 Ma) (Debra, 2001; Dashwood and Abbotts, 1990).

Eogenetic siderite appears to have helped to preserve reservoir quality by supporting the sandstone framework against further mechanical compaction, but mesogenetic calcite considerably reduced primary porosity. The high intergranular volume (IGV) of the sandstones indicates that cementation played a more important role in porosity evolution than mechanical and chemical compaction in both Napo Formation sandstone members. Later dissolution of feldspar grains and siderite cements was the main process of secondary porosity development. Small differences of approximately 1% in the various system tracts are probably within error margins. Hence, primary and secondary porosity are considered to be similar in all the systems tracts, and a relationship with sequence stratigraphy could not be established.

There are however, generally different trends in porosity development in the U and T sandstones. In the U sandstones, remaining average primary porosity is only 10%, while in the underlying T sandstones primary porosity is 13%. The difference is caused by increased calcite cementation in the U sandstones, possibly the result of hydrothermal fluids derived from the limestones which are located between the U and the T units (Figs. 2, 4).

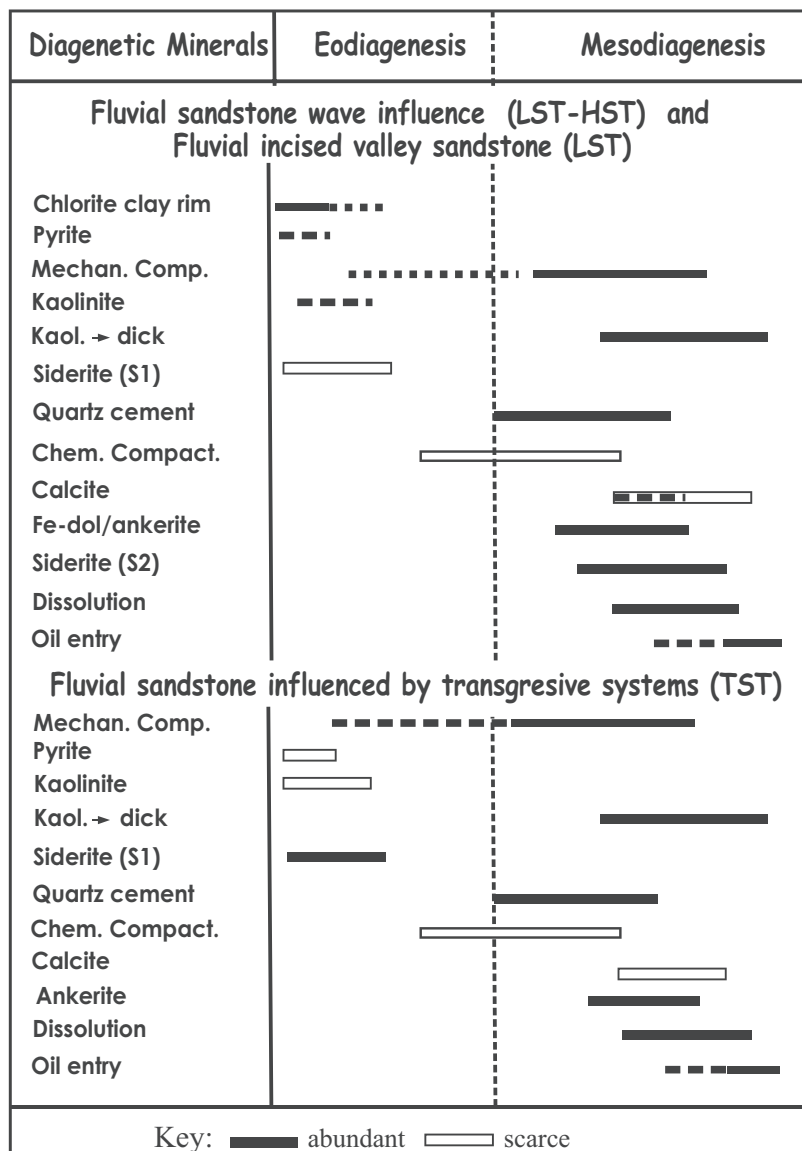


**Fig. 15. Simplified paragenetic sequence of the main diagenetic processes in the U and T reservoir sandstones of the Napo Formation.**

## CONCLUSIONS

Reservoir intervals in the Cretaceous Napo Formation in the Oriente Basin comprise transgressive systems tract (TST), lowstand systems tract - highstand systems tract (LST-HST), and lowstand systems tract (LST) sandstones. The sandstones are composed of fine- to medium-grained quartzarenites and subarkoses cemented by carbonates, quartz, kaolinite-dickite and chlorite with minor pyrite. Early (eogenetic) processes included chlorite grain coating, kaolinite pore filling, and siderite (S1) cementation. Chlorite is absent in TST sandstones but occurred frequently in LST-HST sandstones. Early kaolinite is not present in LST sandstones but was frequent in LST-HST sandstones.

Eogenetic siderite (S1) was partly replaced by later carbonate cements such as siderite S2 and Fe-

dolomite. Although, there appears to be a relationship in the Oriente Basin between the occurrence of S1 siderite and sequence stratigraphy, the nature of the relationship may change when original siderite volumes are considered, because some early siderite has been replaced locally by a later (S2) siderite phase.

The distribution of mesogenetic cements relative to sequence stratigraphy is different in the U and T units. In the U sandstones, calcite is frequent in LST deposits and absent in LST-HST. Fe-dolomite/ankerite is abundant only in the TST deposits. S2 siderite is present in TST and LST deposits but absent in LST-HST. Quartz cement and kaolinite/dickite are equally distributed in all systems tract deposits. In the T sandstones, Fe-dolomite/ankerite is abundant only in the TST, while calcite, quartz and dickite have similar distributions in all systems tracts.

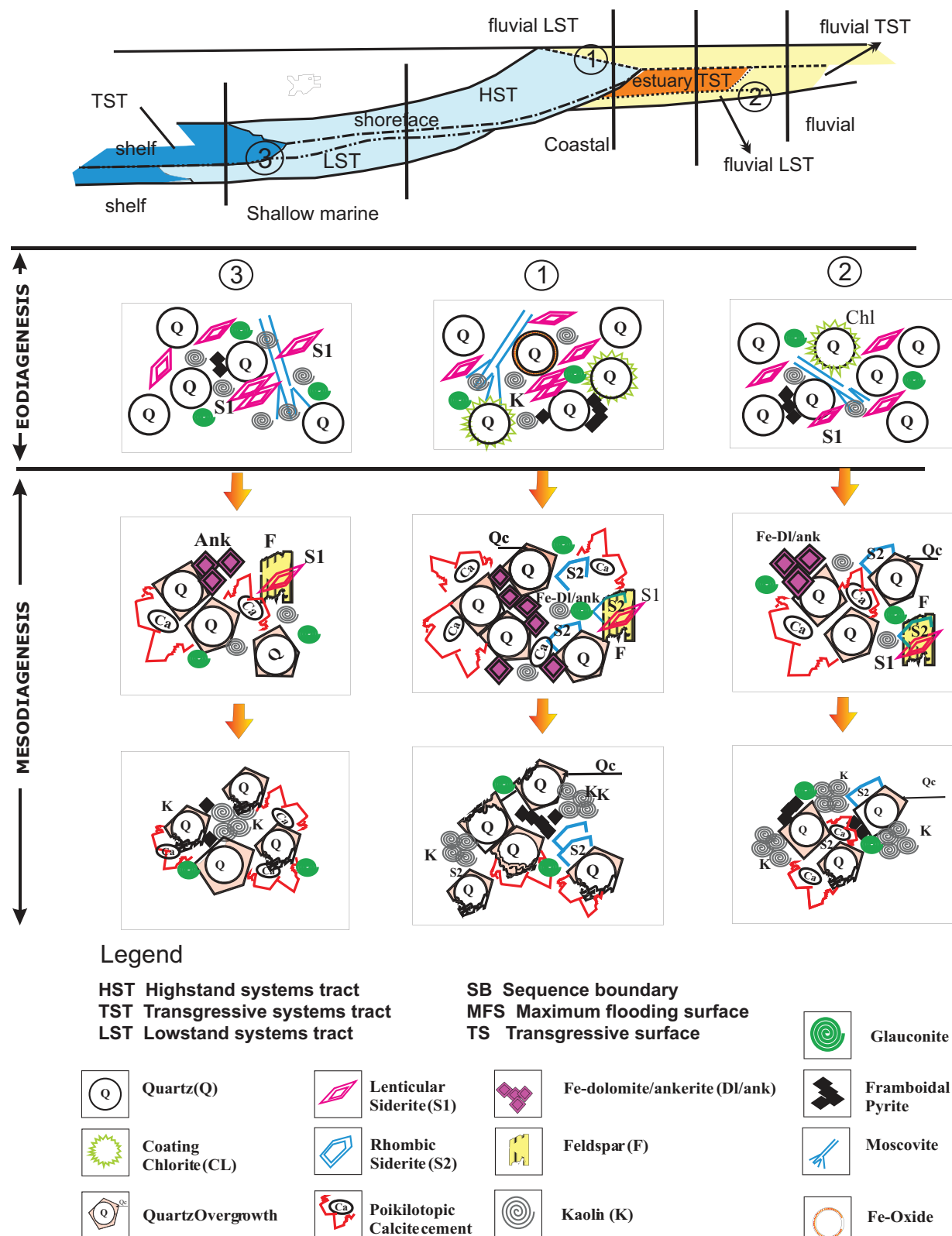


**Fig. 16.** Schematic diagram showing the evolution of principal diagenetic processes in a sequence stratigraphic framework: (1) fluvial sandstones (LST) with wave influence (HST); (2) Fluvial incised valley sandstones (LST); and (3) Sandstones influenced by transgressive systems tract (TST).

Kaolinite cement is interpreted to result from a more intense meteoric-water flux occurring during sea-level fall, whereas chlorite cement may have formed through burial diagenetic transformation of precursor clays e.g. berthierine, which was precipitated in mixed marine-meteoric waters in tidal channel and estuarine environments. The partial replacement of early kaolinite and its recrystallization to dickite may have masked the amount of original early kaolinite; therefore, the relationship to sequence stratigraphy is tentative. Only chlorite seems to have a clear relationship to sequence stratigraphy in the Napo Formation.

The high intergranular volume (IGV) of the sandstones indicates that cementation played a more important role in porosity evolution than mechanical and chemical compaction in both Napo Formation sandstone members. Later dissolution of feldspar grains and siderite cements was the main process of secondary porosity development.

Early chlorite cement helped to retard subsequent pressure solution, and early siderite stabilised the sandstone framework against intense mechanical compaction. These effects are most marked in LST-HST deposits.

Diagenetic studies suggest that the U sandstone is a better reservoir unit than the T sandstone interval. Secondary porosity is approximately twice as high in the U sandstones as in the T sandstones. This is reflected by the different preservation of feldspars in the U and T sandstones, which suggests that leaching of feldspars in the U sandstones was almost twice as severe as in the T sandstone (assuming similar original feldspar contents).

#### ACKNOWLEDGEMENTS

This work was partially funded by Project 01-LECE-EMA 10F of the European Science Foundation, REN2002-11404-E and CGL2006-01861/BTE project of the Spanish Ministry of Science and Technology and the project CCG07-UCM/AMB-2299 of the U.C.M. The authors thank Manuel Rivera from PetroAmazonas bloque 15 (Ecuador), the Dirección Nacional de Hidrocarburos (Ecuador) and ORYX Oil Company (Ecuador) for permission to publish this paper.

The authors are grateful to Antonio Delgado from Laboratorio de isótopos estables (Zaidin, CSIC) for helpful and valuable comments on the isotopic analyses. They acknowledge the valuable help of Elena Vindel from the Department of Crystallography and Mineralogy (UCM) for FI determinations. They also thank D<sup>a</sup> Mariam Barajas, D. Pedro Lozano, D<sup>a</sup> Carmen Valdehita, D. Alfredo Fernandez, D. Juan Luis Baldonado and D. Eugenio Baldonado for technical

assistance at various. They thank Stephen N. Ehrenberg and Hower White for constructive comments on an earlier version which improved the paper. Sadoon Morad is thanked for critical and helpful comments during journal review; JPG editorial staff assisted with the English language presentation.

#### REFERENCES

- AL-AASM, I.S., TAYLOR, B.E. and SOUTH, B., 1990. Stable Isotope analysis of multiple carbonate samples using selective acid extraction. *Chemical Geology*, **80**, 119-125.
- ALMEIDA, J.P., 1986. Estudio de litofacies y del contacto agua petróleo de la Arenisca T del Campo Libertador: Memoria tomo III. *Geología de petróleos Ingeniería de petróleos*, **1**, 119-148.
- BALDOCK, J.W., 1982. Geología del Ecuador. Boletín de la explicación del mapa geológico de la República del Ecuador, scale 1:1000.000. 66 pp.
- BARRAGAN, R.F., CHRISTOPHOUL, H., WHITE, P., BABY, M., RIVADENEIRA, F., RAMIREZ, P. and RODAS, J., 2004. Estratigrafía Secuencial del Cretácico De La Cuenca Oriente Del Ecuador. (Eds) In: La Cuenca Oriente. *Geología y Petróleo*, pp. 45-68.
- BJORLYKKE, K.O., CHUHAN, F.A. and LAUVRAK, O., 1999. Constraints on advective mass transfer during burial diagenesis (Abs.). *AAPG Annual Convention Program*, **8**, A13.
- BURLEY, S.D. and KANTROWICZ, J.D., 1986. Thin section and SEM textural criteria for the recognition of cement dissolution porosity in sandstones. *Sedimentology*, **33**, 587-604.
- CAROTHERS, W.W., ADAM, L.H. and ROSENBAUER, R.J., 1988. Oxygen isotope fractionation between siderite-water and phosphoric acid liberated CO<sub>2</sub>-siderite. *Geochimica et Cosmochimica Acta*, **52**, 2445-2450.
- CHRISTOPHOUL, F. and RIVADENEIRA, M., 1986. Evaluación Geoquímica de Rocas Madres de la Cuenca Amazónica Ecuatoriana: IV Congreso Ecuatoriano de Geología, Minas y Petróleos. Colegio de Ingenieros Geólogos de Minas y Petróleos de Pichincha, **1**, 78.
- COLEMAN, M.L. and RAISWELL, R., 1993. Microbial mineralization of organic matter: mechanisms of self-characterization and inferred rates of precipitation of diagenetic minerals. *Phil. Trans. R. Soc. London*, **344**, 69-87.
- CURTIS, C.D., 1967. Diagenetic iron minerals in some British Carboniferous sediments. *Geochim. Cosmochim. Acta*, **31**, 2109-2123.
- CURTIS, C.D., 1987. Mineralogical consequences of organic matter degradation in sediments: inorganic/organic diagenesis. In: Leggett, J. K. and Zuffa (Eds), *Marine Clastic Sedimentology, Concepts and Case Studies*. Graham and Trotman, London. pp 108-123.
- DASHWOOD, M. F. and ABBOTTS, I. L., 1990. Aspects of the petroleum geology of the Oriente Basin, Ecuador. In: Brooks, J., (Ed.), *Classic petroleum provinces*. *Geol. Soc. Lond. Spec. Pub.*, **50**, 89-117.
- DEBRA, K.H., 2001. The Putumayo-Oriente-Marañón province of Colombia, Ecuador and Peru-Mesozoic-Cenozoic and Paleozoic Petroleum System. *US Geological Survey Digital Data Series*, **63**, 1-35.
- DESBOROUGH, 1978. A biogenic-chemical stratified lake model for the origin of oil shale of the Green River Formation: an alternative to the playa-lake model. *AAPG Bull.*, **89**, 961-971.
- DOTT, R.H. JR, 1964. Wacke, graywacke and matrix - What Approach to Immature sandstone Classification. *Journ. Sedim. Petrol.*, **34**, 625-632.

- DICKINSON, W.R. and SUCZECK, 1979. Plate tectonics and sandstone compositions. *AAPG Bull.*, **63**, 2164 - 2182.
- DICKINSON, W.R., 1985. Interpreting provenance relations from detrital modes of sandstones. In: Zuffa, G.G. (Ed.), *Provenance of Arenites. Series C, Mathematical and Physical Science*, **148**, 333-361.
- EHRENBERG, S.N., 1993. Preservation of anomalously high porosity in deeply buried sandstones by grain-coating clorite: Examples from the Norwegian continental shelf. *AAPG Bull.*, **77**, 1260-1286.
- EHRENBERG, S.N., 1995. Measuring sandstone compaction from modal analyses of thin sections: how to do it and what the results mean. *Journ. Sedim. Res.*, **A65**, 369-379.
- EHRENBERG, S.N., 1989. Assessing the relative importance of compaction processes and cementation to reduction of porosity in sandstone: discussion, compaction and porosity evolution of Pliocene sandstone, Ventura Basin, California: Discussion. *AAPG Bull.*, **73**, 1274-1276.
- EL-GHALI, M.K., MANSURBEG, H., MORAD, S., AL AASM, I. and AJDANLISKY, G., 2006. Distribution of diagenetic alterations in fluvial and paralic deposits within sequence stratigraphic framework: evidence from the Petrohan Terrigenous Group and the Svidol Formation, Lower Triassic, NW Bulgaria.. In: *Diagenesis and Sequence stratigraphic: Predictive Models for Reservoir Quality Evolution of Fluvial and Glaciogenic and Non-glaciogenic, paralic Deposits. Uppsala Universitet paper VII*, pp 1-39.
- ESTUPIÑÁN, J., 2006. Control diagenético sobre la calidad de los reservorios de las arenas U y T de la Fm Napo del Cretácico de la cuenca Oriente, Modelización térmica y su relación con la generación del hidrocarburo. Tesis doctoral. Universidad Complutense de Madrid, 242 pp.
- ESTUPIÑÁN, J., MARFIL, R., DELGADO, A. and PERMANIER, A., 2007. The impact of carbonate cements on the reservoir quality in the Napo Fm Sandstones (Cretaceous Oriente Basin, Ecuador). *Geologica Acta*, **5**, 89-107.
- GAIBOR, J., HOCHULI, P. A., WINKLER, W., and TORO, J., 2005. The Santiago Formation: Source rock of the Napo Group in the Oriente Basin. 6th International Symposium on Andean Geodynamics (ISAG 2005, Barcelona), Extended Abstracts: 290-292.
- GALLOWAY, W.E., 1984. Hydrogeologic regimes of sandstone diagenesis. In: McDonald, D.A. and Surdam, R.C., (Eds.), *Clastic diagenesis. AAPG Memoir*, **37**, 3-13.
- HAYES, J.B., 1979. Sandstone diagenesis-the whole truth. In: P.A. Scholle and P.R. Schluger (Eds.), *Aspect of diagenesis. SEPM Special Publication*, **26**, 127-139.
- HEYDARY, E., 1997. Hydrotectonic models of burial diagenesis in platform carbonates based on formation water geochemistry in North American sedimentary basins. *SEPM Special Publication*, **57**, 53-79.
- HOUSEKNECHT, 1987. Assessing the relative importance of compaction processes and cementation to reduction of porosity in sandstones. *AAPG Bull.*, **71**, 633-642.
- HUDSON, J.D., 1978. Carbon isotopes and limestone cements. *Geology*, **3**, 19-22.
- HUNTER, V.A., 2003. A sequence stratigraphic model of a mixed clastic-carbonate shelf system: the Cretaceous Napo Formation, Oriente Basin, Ecuador, I.
- IRWIN, H. and COLEMAN, M.C., 1977. Isotope evidence for several sources of diagenetic carbonates formed during burial of organic-rich sediments. *Nature*, **269**, 209-213.
- IRWIN, H., 1980. Early diagenetic carbonate precipitation and pore-fluid migration in the Kimmeridge Clay of Dorset, England. *Sedimentology*, **27**, 577-597.
- JAILLARD, E., 1997. Síntesis estratigráfica y sedimentológica del Cretácico y Paleógeno de la Cuenca Oriental del Ecuador. Convenio ORSTOM-PETROPRODUCCION, I, 1-164.
- KETZER, J.M., HOLDZ, M., MORAD, S. and AL-AASM, S., 2003a. Sequence stratigraphic distribution of diagenetic alterations in coal-bearing, paralic sandstones: evidence from the Rio Bonito Formation (early Permian), South Brazil. *Sedimentology*, **50**, 855-877.
- KETZER, J.M., HOLDZ, M., MORAD, S. and AMOROSI, A., 2003b. Predictive Clay Cementation in a sequence stratigraphic framework. In: R. Worden and S. Morad (Eds.), *Clay mineral cements in sandstones. International Association of Sedimentologists Special Publication* **34**, 43-61 pp.
- MATSUMOTO, R. and IIJIMA, A., 1981. Origin and diagenetic evolution of Ca-Mg-Fe carbonates in some coalfields of Japan. *Sedimentology*, **28**, 239-259.
- MORAD, S., 1998. Carbonate cementation in sandstone: distribution patterns and geochemical evolution. *International Association Sedimentology, Special Publication*, **26**, 1-26.
- MORAD, S., KETZER, J. M. and DE ROS, L. F., 2000. Spatial and temporal Distribution of diagenesis alteration in siliciclastic rocks: implications for mass transfer in sedimentary basin. *Sedimentology*, **47**, 95-120.
- MOZLEY, P.S., 1989. Relation between depositional environment and the elemental composition of early diagenetic siderite. *Geology*, **17**, 704-706.
- MOZLEY, P.S. and BURNS, S.J., 1993. Oxygen and carbon isotopic composition of marine carbonate concretions: An overview. *Journal of Sedimentary Petrology*, **63**, 73-83.
- MOZLEY, P.S. and CAROTHERS, W.W., 1992. Elemental and isotopic composition of siderite in the Kuparuk Formation, Alaska: Effect of microbial activity and water sediment interaction on early pore water chemistry. *Journal Sedimentary Petrology*, **62**, 681-692.
- O'NEIL, J.R., CLAYTON, R.N. and MAYEDA, T.K., 1969. Oxygen isotope fractionation in divalent metal carbonates. *Journal of Chemical Physics*, **51**, 5547-5558.
- PAXTON, S.T., SZABO, J.O., AJDUKIEWICZ, J.M. and KLIMENTIDIS, R.E., 2002. Construction of an intergranular volume compaction curve for evaluating and predicting compaction and porosity loss in rigid-grain sandstone reservoirs. *AAPG Bull.*, **86** (12), 2047-2067.
- PETTIJOHN, F.J., POTTER, P.E. and SIEVER, R., 1972. *Sand and sandstone*. Springer-Verlag, 618 pp.
- PITTMAN, E. D., LARESE, R. E. and H.T. HEALD., 1992. Clay coats: Occurrence and relevance to preservation of porosity in sandstones. In: Houseknecht, D.W. and Pittman. (Eds.). *SEPM Spec. Publ.*, **47**, 241-255.
- POSAMENTIER, H.W. and JAMES, D.P., 1993. An overview of sequence-stratigraphic concepts: uses and abuses. In: H.W. Posamentier, C.P. Summerhayes, B.U. Haq and G.P. Allen (Eds.), *Sequence stratigraphy and facies associations*. Oxford, Blackwell, 3-18 pp.
- POSAMENTIER, H.W. and ALLEN, G.P., 1999. Siliciclastic Sequence Stratigraphy- Concepts and Applications. *SEPM, Concepts in Sedimentology and Paleontology Series*, **7**, 210 pp.
- PYE, K., DICKINSON, J.A.D., SCHIAVON, N., COLEMAN, M.L. and COX, M., 1990. Formation of siderite-Mg-calcite-iron sulphide concretions in intertidal marsh and sand flat sediments, North Norfolk. England. *Sedimentology*, **37**, 325-343.
- RAMIREZ, F., PAZOS, J., ROBBS, E. and WHITE, H., 1995. Reservoir Characterization of the Napo Formation Oriente Basin, Ecuador; Part I: Napo A Limestone and U sandstone. Eds, In: Oryx Ecuador Energy Company Quito, Ecuador, 264 pp.
- SCHERER, M., 1987. Parameters influencing porosity in sandstones: A model for sandstones porosity prediction. *AAPG Bull.*, **71**, 485 – 491.
- SCHMIDT, V., and McDONALD, D.A., 1979. The role of secondary porosity in the course of sandstone diagenesis. In: Scholle, A. and Schluger, P.R. (Eds.), *Aspect of diagenesis. SEPM Special Publication*, **26**, 175-207.

- SMITH, J.T. and EHRENBERG, S.N., 1989. Correlation of carbon dioxide abundances with temperature in clastic hydrocarbon reservoir: relationship to inorganic chemical equilibrium. *Marine and Petroleum Geology*, **6**, 129-135.
- SURDAM, R.C., BOESE, S.W. and CROSSEY, L.J., 1984. The chemistry of secondary porosity. In: R.C. Surdam, (Ed.), *Clastic Diagenesis. AAPG Memoir*, **37**, 127-150.
- VAN WAGONER, J.C., MITCHUM, R.M., CAMPION, K.M. and RAHMANIAN, V.D., 1990. Siliciclastic sequence stratigraphy in well logs, cores, and outcrops: concepts for high-resolution correlation of time and facies. *AAPG Methods in Exploration Series*, **7**, 55 pp.
- WHITE, H.J. and BARRAGAN, R., 1997. Reservoir characterization of the Napo Formation, Oriente basin, Ecuador. Part II: Napo T sandstone. *Unpublished report*, Oryx Energy Company, I, 100 pp.
- WHITE, H.J., SKOPEC, R., RAMIREZ, F., RODAS, J. and BONILLA, G., 1995. Reservoir characteristics of Hollín and Napo Formations, western Oriente basin, Ecuador. In: Tankard, A.J., Suárez S.R., and Welsink, H.J. (Eds.), *Petroleum basin of South America. AAPG Memoir*, **62**, 573-596.
- WILSON, M.D., 1994. Reservoir quality assessment and prediction in clastic rocks. *SEPM, Short Course Notes*, **30**, 460 pp.
- WILKINSON, M. and HASZELDINE, R.S., 1996. Aluminium loss during sandstone burial. *Journ. Geol. Soc. London*, **153**, 657-660.
- ZAILTIN, B. A., DALRYMPLE, R. and BOYD, 1994. The stratigraphic organization of incised valley systems associated with relative sea level changes. In: Dalrymple et al. (Eds). *Incised Valley systems: Origin and Sedimentary Sequences. SEPM Special Publication*, **1**, 45-62.